



# Hyperactivation of SREBP induces pannexin-1-dependent lytic cell death

Yanni Xiong<sup>1</sup>, Jie Luo, Zi-Yun Hong<sup>1</sup>, Wen-Zhuo Zhu<sup>1</sup>, Ao Hu<sup>1</sup>, and Bao-Liang Song<sup>1\*</sup>

Hubei Key Laboratory of Cell Homeostasis, College of Life Sciences, Taikang Center for Life and Medical Sciences, Taikang Medical School, Wuhan University, Wuhan, China

**Abstract** Sterol-regulatory element binding proteins (SREBPs) are a conserved transcription factor family governing lipid metabolism. When cellular cholesterol level is low, SREBP2 is transported from the endoplasmic reticulum to the Golgi apparatus where it undergoes proteolytic activation to generate a soluble N-terminal fragment, which drives the expression of lipid biosynthetic genes. Malfunctional SREBP activation is associated with various metabolic abnormalities. In this study, we find that overexpression of the active nuclear form SREBP2 (nSREBP2) causes caspase-dependent lytic cell death in various types of cells. These cells display typical pyroptotic and necrotic signatures, including plasma membrane ballooning and release of cellular contents. However, this phenotype is independent of the gasdermin family proteins or mixed lineage kinase domain-like (MLKL). Transcriptomic analysis identifies that nSREBP2 induces expression of p73, which further activates caspases. Through whole-genome CRISPR-Cas9 screening, we find that Pannexin-1 (PANX1) acts downstream of caspases to promote membrane rupture. Caspase-3 or 7 cleaves PANX1 at the C-terminal tail and increases permeability. Inhibition of the pore-forming activity of PANX1 alleviates lytic cell death. PANX1 can mediate gasdermin- and MLKL-independent cell lysis during TNF-induced or chemotherapeutic reagents (doxorubicin or cisplatin)-induced cell death. Together, this study uncovers a noncanonical function of SREBPs as a potentiator of programmed cell death and suggests that PANX1 can directly promote lytic cell death independent of gasdermins and MLKL.

**Supplementary key words** SREBP • cholesterol • hyperactivation • membrane rupture • Pannexin-1 • apoptosis • gasdermin • lytic cell death

Sterol regulatory element-binding proteins (SREBPs) are transcriptional factors including three isoforms in mammals, namely, SREBP1a, SREBP1c, and SREBP2. All SREBP precursors are composed of an N-terminal transcription factor domain, two hydrophobic transmembrane spans interspaced by a short

luminal loop, and a COOH-terminal domain that binds to SREBP-cleavage activating protein (SCAP). As the master regulator of lipid biosynthesis, the activities of SREBPs are tightly controlled by a well-characterized feedback regulatory mechanism to sense the fluctuation of cholesterol in the endoplasmic reticulum (ER). A high level of cholesterol in the ER facilitates the interaction between SCAP and the ER-residing INSIG proteins. The WD40 domain of SCAP associates with the carboxyl domain of SREBP, thereby restricting the SREBP-SCAP-INSIG trimeric complex in the ER. When the cholesterol level in the ER drops under the threshold, SCAP dissociates from INSIGs and allosterically exposes a hexapeptide motif to be recognized by COPII vesicle components (1, 2). Chaperoning of SREBP to the Golgi apparatus by SCAP allows sequential cleavage by site-1 protease and site-2 protease (S2P), liberating the nuclear form of SREBP (nSREBP). In the nucleus, nSREBP2 activates transcription by binding to sterol response elements (SRE) in the promoter region of target genes (3–8). SREBP1a and SREBP1c preferentially control fatty acid synthesis, and SREBP2 mainly activates cholesterol synthesis although they share a range of overlapping downstream genes.

Malfunctions of SREBPs contribute to the pathogenesis of various metabolic diseases. Increased SREBP1c is associated with insulin resistance in hepatic steatosis. Activated SREBP2 induced the synthesis of hepatic cholesterol, driving the development of non-alcoholic steatohepatitis (9). Previous studies revealed aberrantly increased expression levels of SREBP2 in patients with hepatic steatosis and non-alcoholic steatohepatitis, contributing to the pathogenesis via promoting de novo lipid synthesis (10, 11). Reduction of nuclear forms of SREBPs through SCAP depletion or chemical inhibitor abolished steatosis in insulin-resistant mice (12, 13). Similarly, the knockdown of SCAP protected sucrose-fed hamsters from hypertriglyceridemia, indicating that the SCAP-SREBP2

\*For correspondence: Bao-Liang Song, [blsong@whu.edu.cn](mailto:blsong@whu.edu.cn).

pathway is necessary for developing certain diet-induced metabolic disorders (14).

Many lines of evidence indicate that SREBPs are involved in other biological processes beyond lipid metabolism (3, 15). A genome-wide chromatin immunoprecipitation sequencing (ChIP-seq) from mouse livers showed hepatic SREBP2 binds to the SRE regions of apoptosis and autophagy-related genes, and proved that SREBP2 directly activated autophagy during sterol depletion. Knockdown of SREBP2 during nutrient depletion hindered autophagosome formation and delayed TG mobilization (16). In atheroprone flow-induced atherosclerosis, SREBP2 activation induced NLRP3 inflammasome formation, causing an increase in reactive oxygen species in the endothelium, which facilitated the formation of sclerotic plaques in atheroprone regions of mouse aortas (17). Moreover, overexpression of nSREBP2 in endothelial cells increased atherosclerosis in atherogenic diet-induced *ApoE*<sup>-/-</sup> mice, suggesting a potential connection between SREBP2 transcriptional activity and acute inflammation (17). Previous reports proved that SREBP1a directly activated *Nlrp1a*, which encoded an inflammasome subunit in macrophages. The macrophages from SREBP1a-deficient mice were unable to initiate lipogenesis or activate inflammatory genes under lipopolysaccharide stimulation. Consequently, the SREBP1a-deficient mice had impaired innate immune response toward pathogen challenge (18).

Programmed cell death is essential for the elimination of useless or harmful cells during embryonic development. Apoptosis is immunologically silent by preserving cell integrity, exhibiting chromatin condensation, plasma membrane blebbing, and culminating with the formation of small apoptotic bodies. Apoptotic cells were exposed to a range of “eat me” signals, including phosphatidylserine, and released ATP. These molecules are recognized by macrophages and apoptotic cells are removed via phagocytosis. If scavengers fail to eliminate apoptotic cells promptly, early-stage apoptosis proceeds to a lytic necrotic outcome called secondary necrosis, which is followed by cytoplasmic swelling and rupture of the plasma membrane with induction of inflammatory responses (19–23). Gasdermins are inducers of plasma membrane rupture during pyroptosis. Cleavage by caspases releases N-termini of gasdermins to form oligomerized pores in the plasma membrane with inner diameters of around 10–16 nm, sufficient for cell contents release (23–26). In TNF-induced cell death, the expression of GSDME switched apoptosis to pyroptosis in cancer cells (27). Pyroptosis is a double-edged sword in the context of tumor immunology. Induction of tumor cell pyroptosis by ectopic expression of GSDME or exogenously delivered pore-forming gasdermin protein evoked systemic antitumor response and complete remission of established mammary tumor graft (27, 28). Necroptosis is another type of lytic cell death executed by the pore-

forming MLKL protein. Phosphorylation of MLKL by Receptor-interacting protein 3 (RIP3) induces its membrane localization and disruption of membrane integrity (29). However, whether there are new molecules that damage plasma membrane integrity is unknown.

Previous studies have shown that PANX1 plays a role in apoptosis, inflammasome formation (30, 31), gasdermin-mediated pyroptosis (32) and proinflammatory cytokines secretion (33). Cleavage of C-terminal tail by caspase-3 or caspase-7 induced activation of PANX1. Oligomerization of truncated PANX1 created an ion-channel, with a dilated inner diameter that allows for the release of chemoattractant signals, such as ATP (34–36). Carbenoxolone (CBX), an inhibitor of PANX1, blocks ATP release during apoptosis by clogging the oligomerized PANX1 on the plasma membrane (35, 37). ATP activates P2X7 receptor, leading to the efflux of K<sup>+</sup> across the plasma membrane, a necessary step for forming NLRP3 inflammasome and caspase-1-dependent pyroptosis (31, 38). Although gasdermins have been implicated in the progression of inflammation caused by the activation of PANX1 and P2X7 receptors, it is largely unknown whether PANX1 could directly cause lytic cell death as an executioner.

In this study, we found that nSREBP2 induced lytic cell death by activating transcription factor p73, a homolog of the master cell cycle regulator p53. P73 drove the expression of cell cycle arrest and apoptotic genes and caused subsequent activation of initiator and executioner caspases. The nSREBP2-induced lytic cell death was independent of all known pore-forming proteins, including gasdermin family proteins or MLKL. Unbiased CRISPR screening identified PANX1 as the key protein responsible for cell permeabilization. Genetic ablation of PANX1 in tumor cells blunted TNF-induced lytic cell death. Physiological activation of SREBP2 increased cell sensitivity towards doxorubicin. Our study revealed SREBP2 signaling as a critical regulator of cellular responses to certain stress factors.

## MATERIALS AND METHODS

### Antibodies

The following antibodies were used in this study: rabbit anti-EGFP (Proteintech, 50430-2-AP), mouse anti-β-actin (Sigma, A1978), rabbit polyclonal anti-p53 (Proteintech, 10442-1-AP), rabbit polyclonal anti-p73 (Abclonal, A0385), rabbit anti-caspase-9 (Cell signaling technology, 9502T), rabbit polyclonal anti-caspase-10 (Proteintech, 14311-1-AP), rabbit monoclonal anti-cleaved caspase-3 (Abcam, ab32042), rabbit monoclonal anti-caspase-7 (Cell signaling technology, 12827T), mouse monoclonal anti-caspase-8 (Cell signaling technology, 9746T), rabbit monoclonal anti-GSDME (Abcam, ab215191), rabbit monoclonal anti-GSDMD (Abcam, ab210070), rabbit polyclonal anti-PANX1 (Proteintech, 12595-1-AP), mouse monoclonal anti-cytochrome C (Proteintech, 66264-1-Ig), mouse monoclonal anti-TOM20 (Proteintech, 66777-1-Ig), rabbit monoclonal anti-apaf1 (Cell signaling technology, 8969T), rabbit polyclonal anti-RIP3 (Proteintech, 17563-1-AP).

## Plasmids

The plasmid pLenti-tet-on was a generous gift from Dr Feng Shao (National institute of biological sciences, NIBS). pLenti-tet-on-nSREBP2-EGFP was generated by inserting the human nuclear form of SREBP2 cDNA into vector plasmid pLenti-tet-on, followed by inserting an EGFP epitope-coding DNA. pLenti-tet-on-nSREBP2-5x MYC was generated by replacing EGFP tag with 5xMYC sequence. The human nuclear forms of SREBP1a and SREBP1c were cloned into vector plasmid pLenti-tet-on-EGFP. All nSREBP2 site-directed mutations were generated with ClonExpress one-step cloning kits. pLenti-IRES-caspase-7-puro was generated by inserting human caspase-7 cDNA into vector plasmid pLenti-IRES-puro. pLenti-tet-on-PANX1-FL was generated by inserting human PANX1 cDNA into vector plasmid pLenti-tet-on. The sequence after 1–371 amino acids (aa.) was deleted to generate pLenti-tet-on-PANX1-ΔCTT. pcDNA3-GSDME was generated by inserting human GSDME cDNA into vector plasmid pcDNA3.

## Reagents

Crystal violet, lovastatin, and cycloheximide were purchased from Sigma-Aldrich. 2-Hydroxypropyl-β-cyclodextrin was purchased from Cyclodextrin Technologies Development. Doxycycline hydrochloride (A600889) was purchased from Sangon Biotech. Propidium iodide (P3566) was purchased from Invitrogen. Z-vad (OMe)-FMK (HY16658), Ferostatin-1 (HY100579), and Necrostatin-1s (HY14622A) was purchased from MedChemExpress. Recombinant human TNF (300-01A) was purchased from Peprotech. AZD5582 acetate (T14378L) was purchased from TargetMol. Annexin V-FITC/PI apoptosis detection kit (40302ES60), and Blastidin (60218ES10) were from Yeasen. ClonExpress one step cloning kit (C112-02) was from Vazyme. Lipoprotein-deficient serum (LPDS, density > 1.215 g/ml) was prepared by ultracentrifugation, and delipidated serum (DPS) was prepared by incubating FBS with acetone-washed silicon dioxide to strip non-polar lipids (39, 40).

## Cell culture

HEK-293T cells and HeLa cells were cultured in Dulbecco's Modified Eagle Medium (DMEM, Thermo Fisher Scientific) plus 10% fetal bovine serum (FBS, Gibco) with pen/strep. CHO-7 cells were cultured in a 1:1 mixture of DMEM and Ham's F-12 medium plus 5% FBS with pen/strep. All cells were grown in a humidified chamber at 37°C with 5% CO<sub>2</sub>.

## Immunoblotting analysis

Cells harvest and homogenization were performed as described previously (41). Immunoblots were mixed with 4x loading buffer (12% SDS, 1 M Tris HCl, pH 6.8, 8 M urea, 30% glycerol, 100 mM DTT, 0.02% bromophenol blue, 6% 2-mercaptoethanol) and incubated at 95°C for 5 min. Proteins were resolved on SDS-PAGE and transferred onto PVDF or NC membranes, then blocked with 5% non-fat milk in TBS-T and probed with primary antibodies overnight at 4°C and incubated with secondary antibodies for 1 h at room temperature. Immunoblots were visualized on eBlot.

## Flow cytometry

Cells were treated with dox for the indicated time, then cells were washed with PBS once and labeled with an annexin V-FITC/PI apoptosis detection kit. For detecting the PI signal,

the cells with EGFP tag were treated with dox for the indicated time, after washing with PBS once, incubated with PI for 15–20 min and then analyzed with two channels, EGFP and PI. All cells were analyzed with a flow cytometer (CytoFLEX, Beckman) and data were examined with FlowJo software.

## Cytotoxicity assay

To measure lytic cell death, cells were processed with LDH detection kit (Beyotime, C0017). Cell viability was measured by cell counting kit-8 (TargetMol, C0005) as per the manufacturer's instruction.

## Microscopy imaging of cell death

Live cell imaging for examining cell death morphology was represented in dox-induced pTet-nSREBP2-EGFP HeLa cells. Cells were grown in glass-bottom dishes and treated with or without indicated reagents for 24 h, then the dishes were imaged on the 40x or 63x objective at 10 min intervals for 12 h. Bright-field images and fluorescent images were captured with SP8 confocal microscope (Leica).

## CRISPR-Cas9 knockout cells

Candidate gene-targeting sgRNAs were cloned into LentiGuide-puro vector, then co-transfected with pSPAX and pMD2.G package vectors into HEK-293T cells. The viral medium was collected and mixed with growth medium and supplemented with polybrene to infect pTet-nSREBP2-EGFP HeLa cells which stably expressed Cas9. After 24 h incubation, the infected cells were selected with puromycin. Single-cell clone was screened by seeding with 96-well plate. All gene-knockout cells were examined by sequencing. The sgRNA sequences were as follows: human caspase3 (5'-CATA-CATGGAAGCGAATCAA-3', 5'-AATGGCACAAACATTTGAAA-3'); human caspase7 (5'-TTGAAGGCTATTACTCGTGG-3'); human caspase9 (5'-CGCAGCAGTCCAGAGC ACCG-3'); human caspase10 (5'-ACTGCTGCCACCCGACAAA-3', 5'-GCACCTCAACTGTACCAAAG-3'); human caspase8 (5'-TGATCGACCCTCCGCCAGAA-3'); human GSDMD (5'-TTCCACTTCTACGATGCCA-3'); human GSDME (5'-GTATAACTCAATGACACCGT-3', 5'-TGTCAC-CAAGGACTCCAACG-3'); human GSDMA (5'-CACACTG-GAGCGAGCCGGCA-3'); human GSDMB (5'-AATACGCTGAACATTGCCG-3', 5'-GGATGCCGCACTACACAAC-3'); human GSDMC (5'-CAGCCTCTGTCACCACGTAC-3', 5'-AAGGCGCTGACTCTTCAGAA-3'); human MLKL (5'-GGCAGCCTTGAAGCGTTCA-3'); human PANX1 (5'-GCTGCGAAACGCCAGAACAG-3', 5'-ATCCGAGAACACGTA CTCCG-3'); human APAF1 (5'-TTCCTAAGGAACTCTC-CACA-3', 5'-GTGAAGGTGGAGTACCACAG-3').

## CRISPR-Cas9 screening

Toronto human knockout pooled library (TKO) (42) was a generous gift from Dr Hai Jiang (Center for Excellence in Molecular Cell Science, CAS). To prepare the lentivirus of the library, 2 μg of library DNA was transfected into HEK-293T in the 10-cm dishes with package vectors. After 48 h, lentivirus that covered all sgRNAs was collected by supernatant of infected HEK-293T cells, then filtered by 0.22 μm strainers and stored at –80°C. The titer of lentivirus was measured by cell counting kit-8. To get 100-fold coverage, 6 × 10<sup>7</sup> Tet-on HeLa cells were infected with the lentivirus at MOI of 0.3. 24 h after infection, the medium was changed to normal cell

growth, then cells were re-seeded with a growth medium containing 4  $\mu\text{g/ml}$  puromycin for an additional 24 h. Survival cells were routinely passaged and maintained the 100-fold coverage, the half  $6 \times 10^7$  cells were regarded as control samples, the other cells were treated with 0.3  $\mu\text{g/ml}$  dox for 36 h, then preloaded with PI for 15 min, cells that contained negative PI signal and positive EGFP signal were collected by FACS. The enriched cells were used as candidate genes for deep sequencing.

### RNA-sequencing

Cells in 60 mm dishes were treated with or without 0.3  $\mu\text{g/ml}$  dox for 8 h and 16 h, then were extracted for RNA isolation and marked as T1, T2, T3, and T1 as no-treatment wild-type cells. Every sample was repeated twice. All RNA samples were under quality control and used for Hiseq sequencing. For RNA-seq analysis, the clean reads were obtained by filtering raw data and aligned to the human reference genome. Differential gene expression analysis was performed by GO and KEGG. Genes were regarded as differentially expressed when the  $\log_2$  of the fold change  $> 1$  and  $P$  value  $< 0.05$ .

### siRNA knockdown

Two siRNA targets TAp73 and  $\Delta\text{Np73}$  were designed as former reports (43) and synthesized by RiboBio. Cells were transfected with individual siRNA and Lipofectamine RNAiMAX reagent (Invitrogen, 13778075) following the manufacturer's recommendations. The siRNA sequences were used as follows:

siTAp73: 5'- AACGGAUUCAGCAUGGACGU-3'  
si $\Delta\text{Np73}$ : 5'- AACCCUCGCCACGGCCAGUUC-3'

### Quantitative PCR

Cells in 60 mm dishes were treated according to indicated conditions. Total RNAs were extracted by TRIzol (Thermo Fisher Scientific), 1  $\mu\text{g}$  RNA was subjected to reverse transcription with HiScript II reverse transcriptase and indicated buffer (Vazyme, R201). Quantitative PCR (qPCR) was conducted with Hieff qPCR SYBR Master Mix (High ROX) (Monad, MQ10301S) on a Bio-Rad CFX96 or CFX384. Human *GAPDH* was used as control. The primer sequences were listed in supplemental Table S1.

### Statistics

All statistical data were analyzed with the GraphPad Prism software. Data were expressed by mean  $\pm$  SD and analyzed by unpaired two-tailed Student's  $t$  test.  $P$  value  $< 0.05$  was regarded as significant data.

## RESULTS

### nSREBP2 overexpression induces lytic cell death

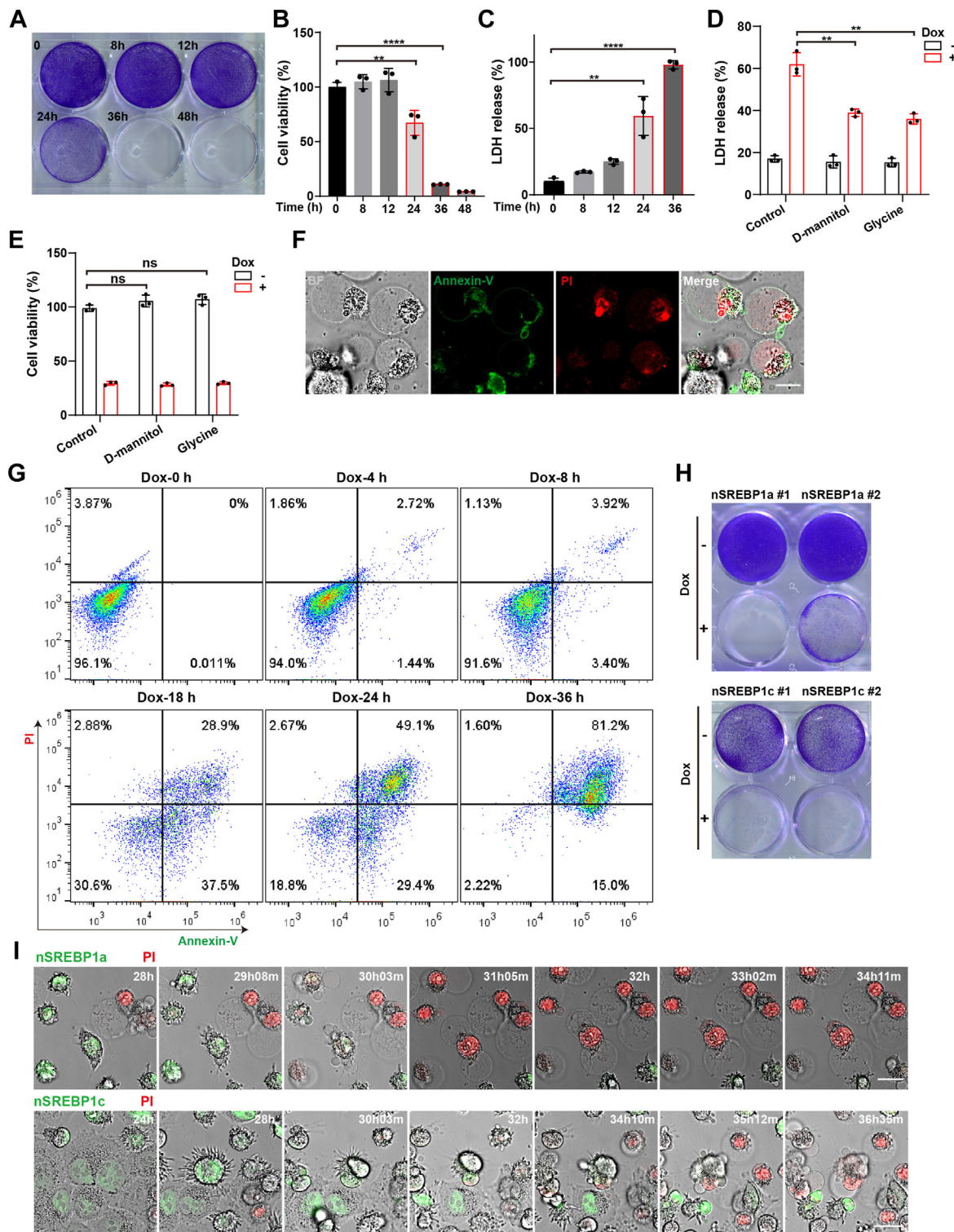
We accidentally found that overexpression of nSREBP2 might cause cell death since we were unable to establish a cell line stably expressing nSREBP2. To validate this hypothesis, we generated HeLa cells stably expressing nSREBP2 under the control of a doxycycline (dox)-inducible promoter (HeLa/pTet-nSREBP2-EGFP). Induction of nSREBP2 by dox resulted in massive death in HeLa/pTet-nSREBP2-EGFP (Fig. 1A), but not the parental HeLa cells (supplemental

Fig. S1A–C). A similar experiment was performed in several different cell lines, including MO3.13, NIH3T3, and CHO-7. Overexpression of nSREBP2 caused similar patterns of cell death in these cells (supplemental Fig. S1D). Upon dox treatment, HeLa/pTet-nSREBP2-EGFP cells gradually lost the viabilities and increased membrane permeabilities, evidenced by increased lactate dehydrogenase (LDH) in the cell culture supernatant (Fig. 1B, C). Osmotic-protectants such as D-mannitol or glycine prevented cells from LDH release but failed to rescue cell death (Fig. 1D, E). To define the phenotype of nSREBP2-induced cell death, we probed dox-treated cells with Annexin-V and propidium iodide (PI), which recognize exposed phosphatidylserine (PS) and intracellular nucleic acids, respectively. Flow cytometry indicated that PS externalization and membrane disintegration occurred simultaneously, suggesting a process of lytic cell death (Fig. 1G). Concordantly, balloon-like membrane extrusions were clearly observed after nSREBP2 induction (Fig. 1F and supplemental Video S1). The lysis-induction capacity of nSREBP2 was dependent on its transcription activity and nuclear localization, as transcription activity-null mutant (Y342R) or nucleus-excluded mutant (R371E/K372E) forms of nSREBP2 failed to induce cell death (supplemental Fig. S2A–D). In addition, the nSREBP2 mutant lacking DNA binding domain (329–354 aa) failed to induce lytic cell death (supplemental Fig. S2E, F). Dox-induced overexpression of two related homologs of SREBP2, namely nSREBP1a and nSREBP1c, caused lytic cell death with a similar pattern (Fig. 1H, I, supplemental Videos S2, and S3).

Overexpression of nSREBP2 induced the expression of cholesterol biosynthetic genes, the lethal level of nSREBP2 transcription activity is higher than the physiological one upon sterol depletion (supplemental Fig. S3A). To exclude the possibility that nSREBP2-induced cell death is through cholesterol overload (44, 45), we inhibited endogenous cholesterol synthesis by blocking the rate-limiting enzyme HMGCR using lovastatin, or depleted cellular cholesterol using hydroxypropyl- $\beta$ -cyclodextrin along with lipoprotein/lipid-deficient serum. None of these interventions rescued cells from nSREBP2-induced cell death (supplemental Fig. S3B, C), suggesting a lipid metabolism-independent mechanism.

### Transcriptional activation of apoptotic and cell cycle arrest-associated genes by nSREBP2

To explore the downstream effector through which nSREBPs induced cell death, we compared the differentially expressed genes (DEGs) in cells with or without dox treatment by bulk RNA sequencing. DEGs from two independent experiments were plotted, and they showed a highly repetitive expression signature, with a coefficient of determination ( $R^2$ ) of 0.865. Among these upregulated genes, several well-established SREBP2 target genes, such as low-density lipoprotein receptor



**Fig. 1.** nSREBP2 overexpression induces lytic cell death. A: time curve of 0.3  $\mu\text{g/ml}$  doxycycline (dox) treatment in HeLa-pTet-nSREBP2 cells. Cells were treated with dox for the indicated time and analyzed by crystal violet staining. B and C: quantification of cell viability of tet-on-nSREBP2 cells. Cells were treated with 0.3  $\mu\text{g/ml}$  dox for the indicated time and analyzed by cell counting kit-8 (B) or LDH test (C). Data are presented as means  $\pm$  SD. Statistical analyses, unpaired two-tailed Student's *t* test. D and E, HeLa-pTet-nSREBP2 cells were treated with 0/0.3  $\mu\text{g/ml}$  dox plus control, 25 mM D-mannitol or 10 mM glycine for 30 h, LDH (D) and cell viability (E) were tested. Data are presented as means  $\pm$  SD. Statistical analyses, unpaired two-tailed Student's *t* test. F, Time-lapse confocal images of HeLa-pTet-nSREBP2-5xMYC cells were taken at the indicated time points after 0.3  $\mu\text{g/ml}$  dox induction for 36 h. Real time videos are included in [supplemental Video S1](#). Scale bar, 25  $\mu\text{m}$ . G, Annexin V/PI flow cytometric analysis of dox-induced cell death phenotype. H, Two clones of HeLa-pTet-nSREBP1a/c cells and HeLa-pTet-nSREBP2 cells were treated with or without 0.3  $\mu\text{g/ml}$  dox for 36 h. Cell viability was analyzed by crystal violet staining. I, Time-lapse confocal images of HeLa-pTet-nSREBP1a/c cells. HeLa-pTet-on-nSREBP1a/c cells were induced by 0.3  $\mu\text{g/ml}$  dox for 24 h, preloaded with 10  $\mu\text{g/ml}$  PI for 15 min, then imaged at 40 $\times$  magnification at 5 min intervals for 12 h. Real time videos are included in [supplemental Videos S2](#) and [S3](#). Scale bar, 25  $\mu\text{m}$ . \*\*  $P < 0.01$ , \*\*\*  $P < 0.001$ , ns, not significant.

(*LDLR*), 3-hydroxy-3-methylglutaryl-coenzyme A reductase (*HMGCR*), lanosterol synthase (*LSS*), insulin-induced gene 1 (*INSIG1*), were significantly enriched, implying highly active sterol biosynthesis pathway (Fig. 2A).

Kyoto Encyclopedia of Genes and Genomes (KEGG) analysis revealed the clustering of several pathways related to cell death, including p53 signaling, cell cycle, and apoptosis (Fig. 2B). Indeed, expression analysis of individual genes involved in cell cycle regulation showed an increased transcription level of anti-proliferative genes, including the tumor suppressor *CDKN1C* and *CDKN1A*. These expression patterns were further verified by quantitative PCR (qPCR). In contrast, pro-proliferative genes were negatively enriched, such as *CCND1* and *MYC*, whose amplification is observed in various cancer types (46) (Fig. 2C, D). Induction of nSREBP2 expression by dox for 12 h dramatically upregulated the protein level of p21 and p57 (encoded by *CDKN1A* and *CDKN1C* respectively), implying the activation of p53 signaling and the status of immediate cell cycle arrest (Fig. 2E).

Meanwhile, the RNA-seq and qPCR data suggested upregulated gene clusters related to cell apoptosis, such as *TP53INP1* and *TP53INP2*, which are also well-recognized downstream targets of p53, were enriched after 8 h of dox treatment. Upregulation of pro-apoptotic expression signatures was observed in 8 h, confirmed by RNA-seq and qPCR (Fig. 2F, G). Moreover, cell fractionation revealed a substantial level of cytochrome C released from mitochondria, indicating a central event in apoptosis initiation (Fig. 2H).

### p73 is activated at the transcriptional level during nSREBP2 overexpression

We found that p73, a functional homolog of p53, was significantly upregulated after nSREBP2 activation (Fig. 3A). p73 belongs to the p53 family that targets apoptosis and induces cell cycle under DNA damage stimulation. p73 has multiple transcript isoforms. The N-terminal transactivation domain-containing isoform (TAp73) exhibits p53-like transcriptional activity, while the N-terminal deleted isoforms ( $\Delta$ Np73) are dominant negative in the context of pro-apoptotic functions (47–49). Immunoblot analysis showed that the TAp73 isoform, but not the  $\Delta$ Np73 species was activated after dox treatment (Fig. 3B, C). Similar regulation of p73 isoforms was observed during cholesterol depletion, which activated endogenous SREBP2 in physiological conditions (Fig. 3D). To validate the function of these isoforms during nSREBP2-induced cell death, we utilized siRNA targeting the specific sequences of these transcripts. Knockdown of the active TAp73 resulted in less cell death, as evidenced by decreased LDH release and reduced cleavage of caspase-9, whereas silencing  $\Delta$ Np73 showed no impact (Fig. 3E, G). We further generated p73 knockout cells by CRISPR-Cas9 technique. HeLa cells deficient in p73 were highly resistant

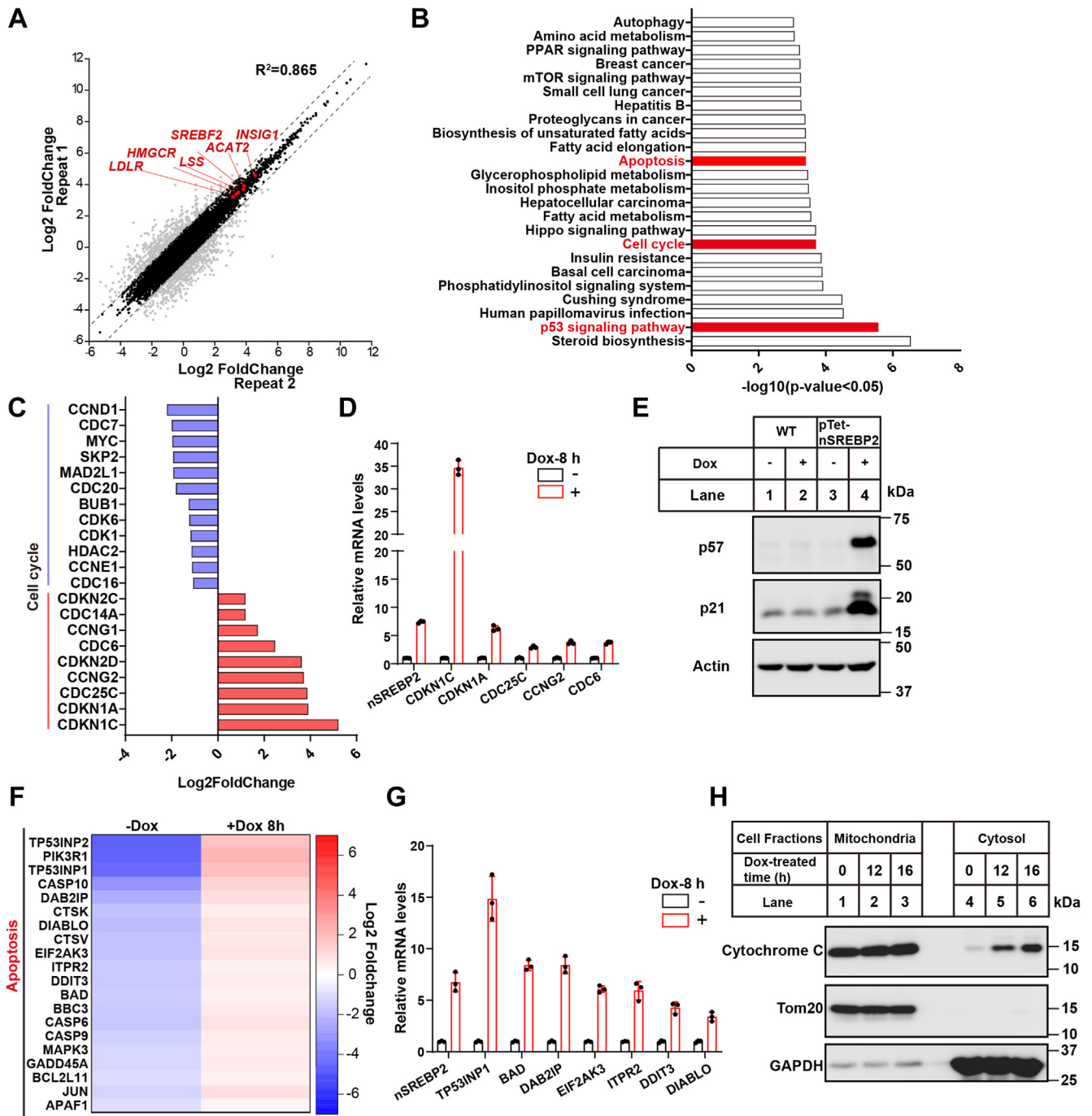
to nSREBP2-triggered cell content release and lytic cell death (Fig. 3H–J). These results proved that transcription activity of p73 was required for nSREBP2-induced lytic cell death.

### nSREBP2 triggers cell death in a caspase-dependent manner

We next sought to define the mode of cell death induced by nSREBP2. We employed well-established small molecule inhibitors of apoptosis, ferroptosis, and necroptosis to dissect their contributions, respectively. The pan-caspase inhibitor z-VAD (50) completely blocked nSREBP2-induced cell death (Fig. 4A). Cell morphology remained nearly normal after 36 h of nSREBP2 expression in the presence of z-VAD (Fig. 4B). Proteolytic activation of the initiator caspases, namely, caspase-9 and caspase-10, was observed after nSREBP2 induction (Fig. 4C), concordant with previously observed cytochrome C release (Fig. 2H). Double knockout of *caspase-9* and *caspase-10* resulted in resistance to nSREBP2-induced LDH release and cell death (Fig. 4D and supplemental Fig. S4A). Consequently, active forms of the executioner caspases, namely caspase-3 and caspase-7 (51), were detected following dox treatment (Fig. 4E). This process was dependent on caspase-9 and caspase-10. Deletion of *caspase-9* and *caspase-10* completely inhibited activation of caspase-3 and caspase-7 (supplemental Fig. S4B). Deletion of both *caspase-3* and *-7* prevented nSREBP2-induced cell death, whereas ablation of caspase-3 alone was insufficient (Fig. 4F–H). PI staining also confirmed double knockout of *caspase-3* and *caspase-7* maintained the integrity of membranes (Fig. 4I and supplemental Video S4). Overexpression of caspase-7, but not its catalytic dead form (C186A), re-sensitized the double knockout cells to nSREBP2-induced cell death (Fig. 4J–K). We found that caspase-8 was dispensable, although a cleaved, active form of caspase-8 was observed under dox treatment (Supplemental Fig. S4B and S5A–C). These results highlighted the role of apoptotic caspases in nSREBP2-induced lytic cell death. But how these caspases caused membrane rupture remains unanswered.

### nSREBP2-induced lytic cell death is independent of gasdermins or MLKL

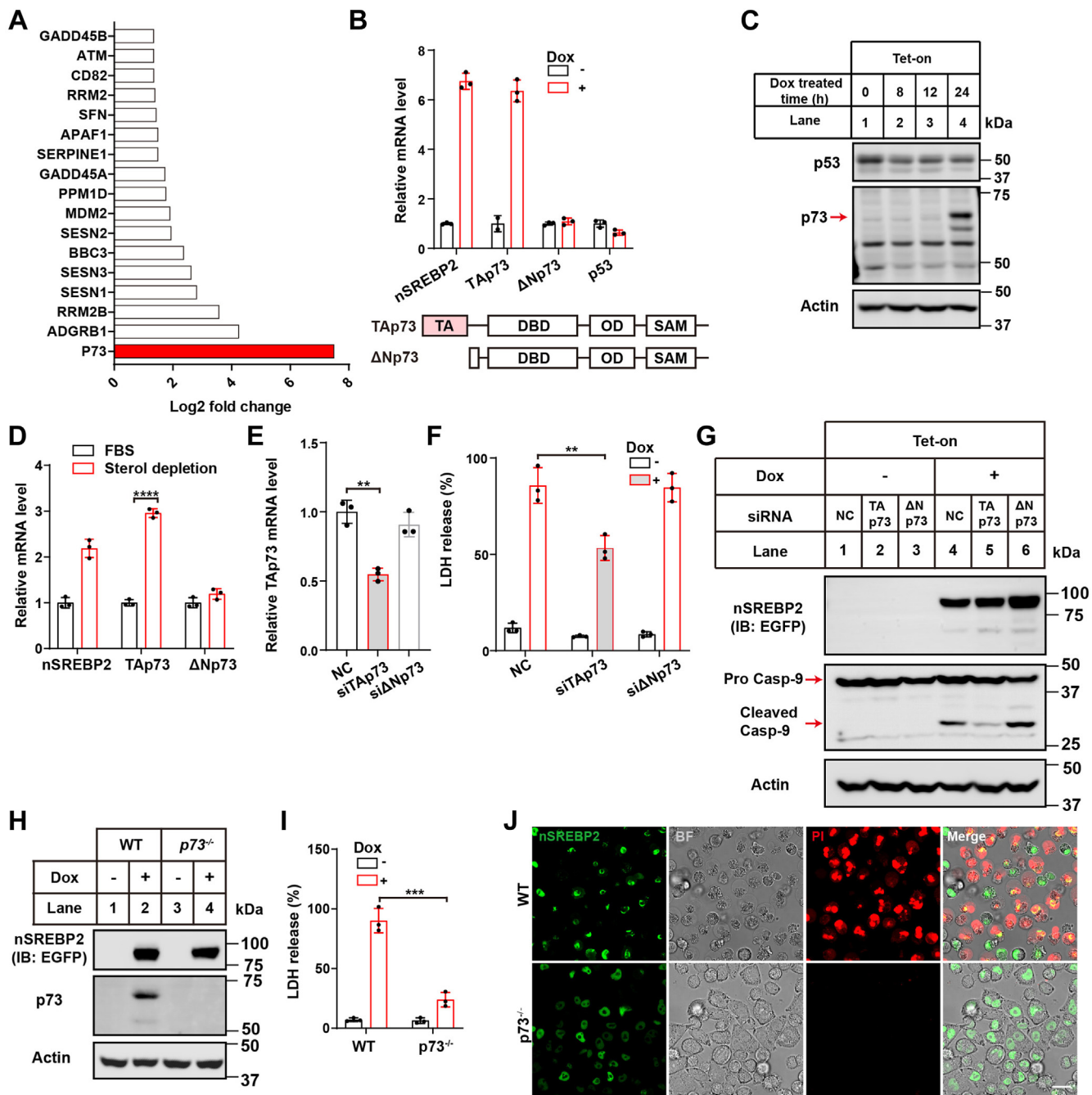
Typical apoptotic morphologies, including cell shrinkage and membrane blebbing, were clearly distinct from the pyroptotic phenotype during nSREBP2 activation. We noticed that GSDME was activated upon nSREBP2 activation, but knockout of GSDME failed to prevent cells from nSREBP2-induced lytic death (supplemental Fig. S6A–E). To identify key components in this process, we evaluated the contribution of the well-established gasdermin family by generating a gasdermin A, B, C, D, and E panto-knockout cell line (supplemental Fig. S7A–C, designated as ABCDE-5KO). Gasdermin proteins share



**Fig. 2.** Transcriptional activation of apoptotic and cell cycle arrest-associated genes upon nSREBP2 induction. **A:** RNA-seq analysis of dox-induced HeLa-pTet-nSREBP2 cells. Cells were treated with 0 or 0.3  $\mu\text{g}/\text{ml}$  dox for 8 h. **B:** KEGG results for upregulated pathways using dox inducible genes from **A**. **C:** Cell cycle pathway analysis from **B**. **D:** QPCR analysis of cell cycle-related genes. Data are represented as mean  $\pm$  SD. **E:** Western blotting analysis was used to detect the expression of p21 and p57 with or without the induction of nSREBP2. HeLa and HeLa-pTet-nSREBP2 cells were treated with 0/0.3  $\mu\text{g}/\text{ml}$  dox for 16 h. **F:** Heatmap of representative apoptosis-related genes from **B**. **G:** QPCR analysis of apoptosis-related genes. Data are represented as mean  $\pm$  SD. **H:** Immunoblot of cytochrome C, Tom20, and GAPDH in HeLa-pTet-nSREBP2 cells. Cells were treated with or without 0.3  $\mu\text{g}/\text{ml}$  dox for 12 h and 16 h. Mitochondria and cytosol fractions were separated for immunoblotting.

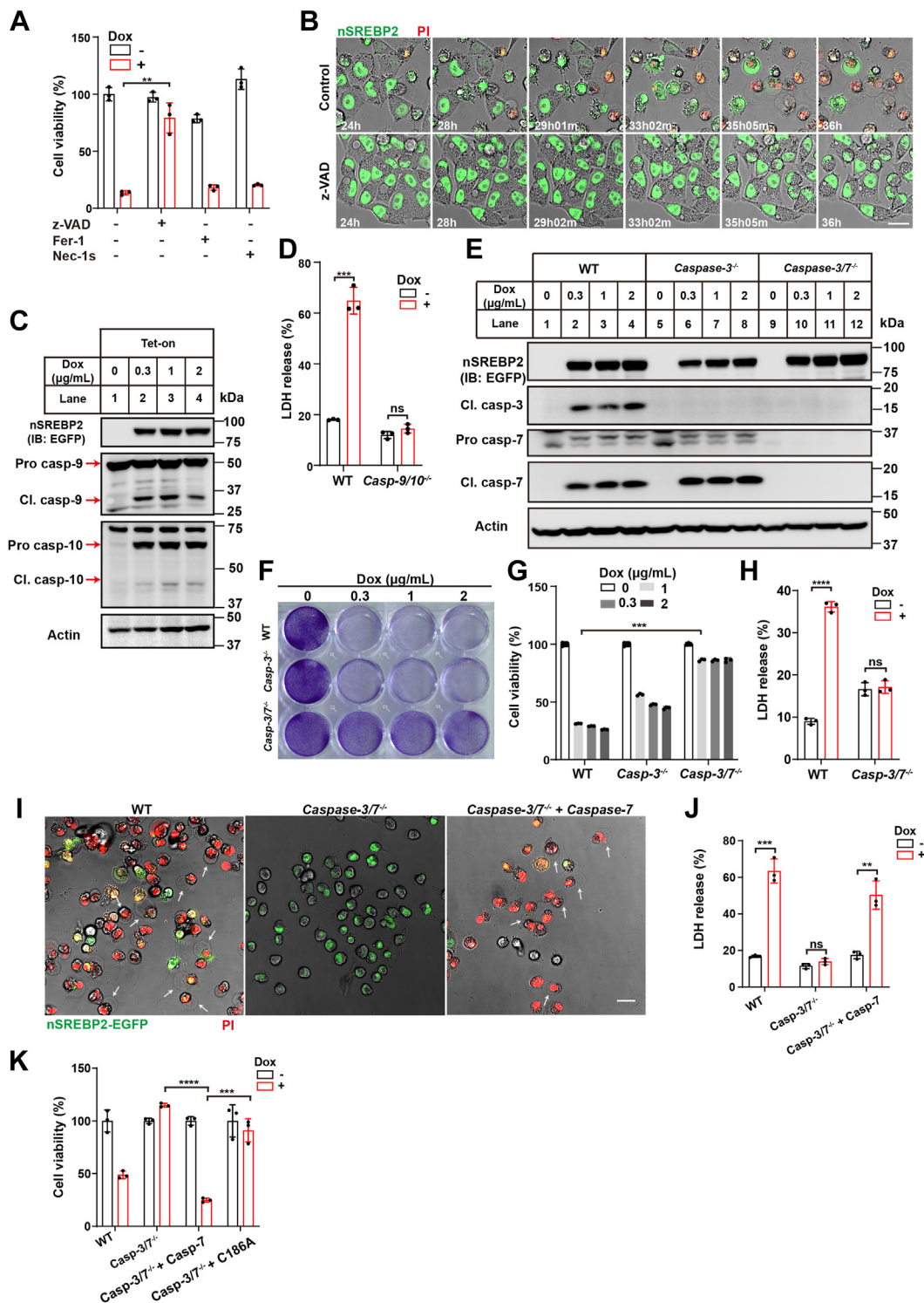
common pore-forming capacities on cell membranes via oligomerization (26). Surprisingly, ABCDE-5KO cells still underwent nSREBP2-induced cell death (Fig. 5A), suggesting that gasdermins were not the executioner in this process.

To test whether MLKL participated in the process of nSREBP2-induced cell death, we generated an MLKL-deficient cell line via CRISPR-Cas9 technique (supplemental Fig. S7D). MLKL-deficient cells expressed comparable level of nSREBP2 to WT cells

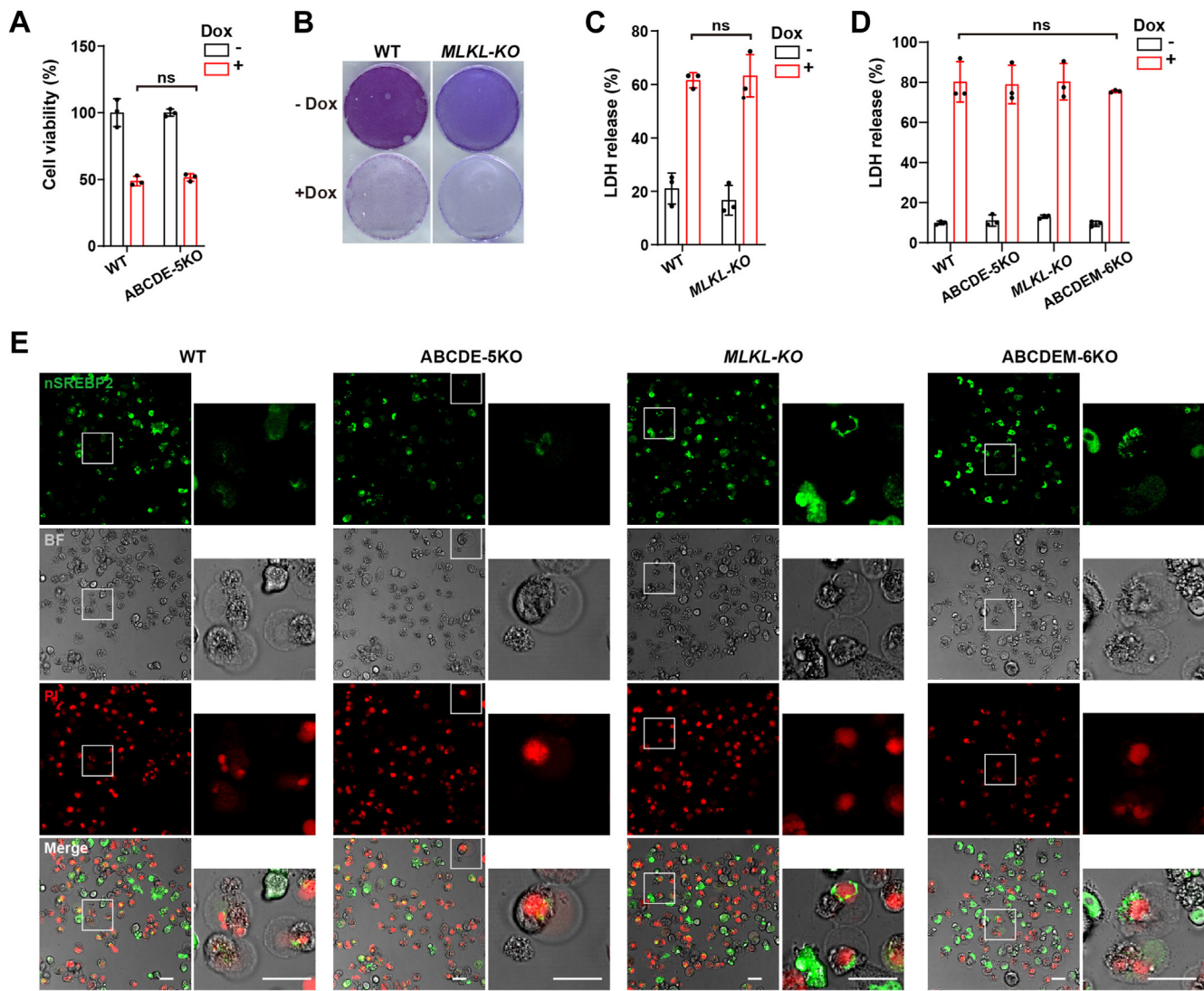


**Fig. 3.** Ablation of p73 prevents the nSREBP2-induced lytic cell death. **A:** Overexpression of nSREBP2 increased gene transcription of p53 pathway. **B:** QPCR analysis of p73 transcripts. Cells were treated with or without 0.3  $\mu\text{g}/\text{ml}$  dox for 16 h, then RNA was harvested for QPCR analysis. The diagram below showed two transcripts of p73, TAp73 and  $\Delta\text{N}$  p73. Data are presented as means  $\pm$  SD. **C:** Western blotting analysis was used to detect the expression of p73 and p53 with the induction of nSREBP2. HeLa-pTet-nSREBP2 cells were treated with or without 0.3  $\mu\text{g}/\text{ml}$  dox for indicated time, then harvested for Western blot analysis. **D:** QPCR analysis of nSREBP2 and p73 transcripts. HeLa-pTet-nSREBP2 cells were cultured in 10% FBS or sterol depletion medium (5% lipoprotein-deficient serum, 1  $\mu\text{M}$  lovastatin, 10  $\mu\text{M}$  mevalonate) for 24 h and then subjected to analysis. **E:** QPCR analysis of p73 siRNA knock-down efficiency. Data are presented as means  $\pm$  SD. Statistical analyses, unpaired two-tailed Student's *t* test. **F:** LDH release test. HeLa-pTet-nSREBP2 cells were transfected with indicated siRNA for 24 h, then treated with 0.3  $\mu\text{g}/\text{ml}$  dox for 24 h. Lytic cell death was measured by LDH in the medium. Data are presented as means  $\pm$  SD. Statistical analyses, unpaired two-tailed Student's *t* test. **G:** The effect of p73 siRNA on nSREBP2 expression and caspase-9 cleavage. **H:** Immunoblotting analysis of WT and p73 knockout HeLa-pTet-nSREBP2 cells. **I:** LDH test identified the effect of p73 knockout on nSREBP2 induction. Data are presented as means  $\pm$  SD. Statistical analyses, unpaired two-tailed Student's *t* test. **J:** representative images of WT and p73 knockout HeLa-pTet-nSREBP2 cells. All cells were treated with 0.3  $\mu\text{g}/\text{ml}$  dox for 36 h. Cells were preloaded with 10  $\mu\text{g}/\text{ml}$  PI for 15 min and imaged at 63 $\times$  magnification. Scale bar, 25  $\mu\text{m}$ .  $**P < 0.01$ ,  $***P < 0.001$ ,  $****P < 0.0001$ .





**Fig. 4.** nSREBP2 triggers cell death in a caspase-dependent manner. A: effects of different cell death inhibitors on dox-induced cell death. HeLa-pTet-nSREBP2 cells were treated with or without 0.3  $\mu\text{g/ml}$  dox and inhibitors for 24 h. Cell viability was analyzed by CCK8. z-VAD (z-VAD-FMK), 50  $\mu\text{M}$ ; Fer-1 (ferrostatin-1), 38  $\mu\text{M}$ ; Nec-1s (necrostatin-1s), 30  $\mu\text{M}$ . Data are presented as means  $\pm$  SD. Statistical analyses, unpaired two-tailed Student's *t* test. B: representative images of HeLa-pTet-nSREBP2 cells treated with or without z-VAD. All cells were treated with or without 50  $\mu\text{M}$  z-VAD and with 0.3  $\mu\text{g/ml}$  dox for 24 h, then imaged at 40 $\times$  magnification at 5 min intervals for 12 h. Scale bar, 25  $\mu\text{m}$ . C: effects of dox induction on intracellular processing of caspase-9 and caspase-10. D: effects of caspase-9/10 on dox-induced cell death. WT and caspase-9/10 double deficient HeLa-pTet-nSREBP2 cells were treated with or without 0.3  $\mu\text{g/ml}$  dox for 36 h, and lytic cell death was analyzed by LDH. Data are presented as means  $\pm$  SD. Statistical analyses, unpaired two-tailed Student's *t* test. E: immunoblotting of caspase-3 and caspase-7 expression on dox induction in WT, caspase-3 deficient and caspase-3/7 double-deficient HeLa-pTet-nSREBP2 cells. F: Crystal violet staining. G: quantification of cell viability in F. H: effects of caspase-3 and 7 on dox-induced lytic cell death were analyzed by LDH tests. Data are presented as means  $\pm$  SD. Statistical analyses, unpaired two-tailed Student's *t* test. I: representative images of the effect of caspase-7 overexpression on caspase-

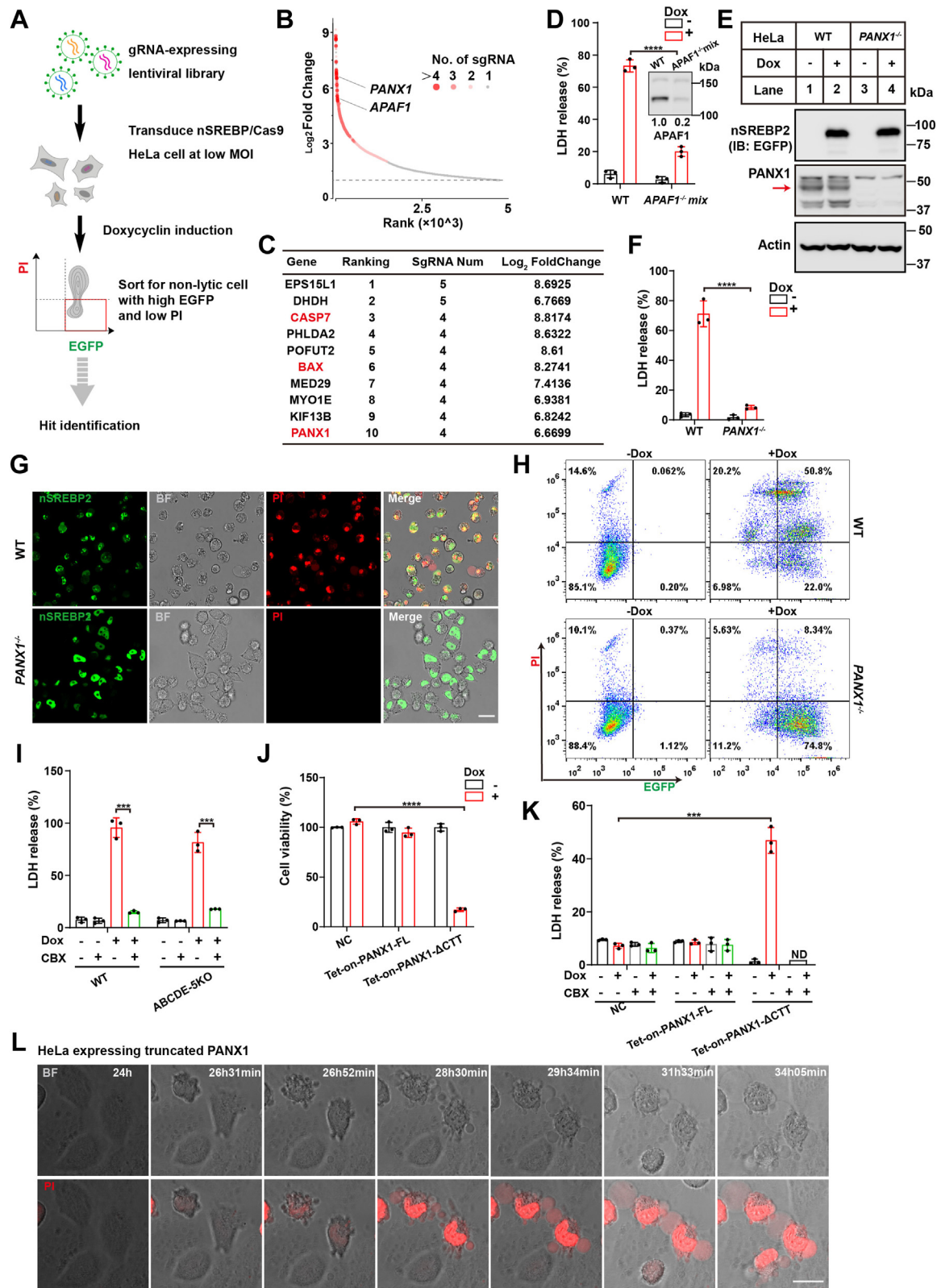


**Fig. 5.** nSREBP2 induced lytic cell death is independent of gasdermins or MLKL. A: cell viability of WT and ABCDE-5KO HeLa-pTet-nSREBP2 cells were analyzed by cell counting kit-8. WT and ABCDE-5KO HeLa-pTet-nSREBP2 cells were treated with or without 0.3  $\mu\text{g}/\text{ml}$  dox for 24 h. Data are presented as means  $\pm$  SD. Statistical analyses, unpaired two-tailed Student's *t* test. B: Crystal violet staining of the effects of *MLKL-KO* in HeLa-pTet-nSREBP2 cells. C: Dox-induced expression of nSREBP2 caused LDH release in both WT and *MLKL-KO* cells. D: LDH release test. E: representative confocal images of WT, ABCDE-5KO and *MLKL-KO*, and ABCDEM-6KO HeLa-pTet-nSREBP2 cells. All cells were induced by 0.3  $\mu\text{g}/\text{ml}$  dox for 24 h, then imaged at 40 $\times$  magnification at 5 min intervals for 12 h. Scale bar, 25  $\mu\text{m}$ . Real-time videos are included in [supplemental Video S5](#). ns, not significant.

upon dox induction ([supplemental Fig. S7E](#)). However, knockout of MLKL did not protect cells from nSREBP2-induced lytic death ([Fig. 5B, C](#)). We also generated gasdermins and MLKL hexa-knockout cell lines (designated as ABCDEM-6KO). Gasdermins deficiency was confirmed by their resistance to lipopolysaccharide (LPS) priming followed by nigericin

treatment ([supplemental Fig. S7F](#)), while MLKL-deficiency was indicated by the lack of sensitivity to TNF/Smac mimetic/z-VAD induced necroptosis in the presence of RIP3 ([supplemental Fig. S7G, H](#)). We proved that ABCDEM-6KO cells released a substantial amount of LDH as other cells ([Fig. 5D](#)). Time-lapse imaging captured balloon-like structures in both

3/7 double-deficient HeLa-pTet-nSREBP2 cells. The caspase-3/7 double-deficient HeLa-pTet-nSREBP2 cells were pre-infected with or without caspase-7 expression lentivirus, all cells were treated with 0.3  $\mu\text{g}/\text{ml}$  dox for 24 h, then imaged at 40 $\times$  magnification at 5 min intervals for 12 h. All cells were preloaded with 10  $\mu\text{g}/\text{ml}$  PI for 15 min. Real-time videos are included in [supplemental Video S4](#). Scale bar, 25  $\mu\text{m}$ . J: the effect of caspase-7 overexpression on caspase-3/7 double-deficient HeLa-pTet-nSREBP2 cells. The caspase-3/7 double-deficient HeLa-pTet-nSREBP2 cells were pre-infected with or without caspase-7 expression lentivirus, all cells were treated with or without 0.3  $\mu\text{g}/\text{ml}$  dox for 36 h. Lytic cell death was analyzed by LDH test. K: WT and caspase-3/7-deficient HeLa-pTet-nSREBP2 cells were infected with or without wild-type and mutated caspase-7 (C186A). Cell viability was analyzed by CCK8. ns, not significant, \*\*  $P < 0.01$ , \*\*\*  $P < 0.001$ , \*\*\*\*  $P < 0.0001$ .



**Fig. 6.** Requirement of PANX1 as the mediator for nSREBP2-induced membrane rupture. **A:** scheme depicting the screening of PANX1 as the mediator for nSREBP2-induced cell death. The Caspase-3-deficient HeLa-pTet-nSREBP2 cells were used for CRISPR/cas9 screening. **B:** genes were ranked according to the enrichment of sgRNA counts. The dotted line represents a fold change of 2. **C:** the list of top 10 genes from **B**. **D:** The nSREBP2 expression-induced LDH release in WT and APAF1-deficient HeLa-pTet-nSREBP2 cells. WT and APAF1-deficient HeLa-pTet-nSREBP2 cells were treated with 0/0.3  $\mu$ g/ml dox for 36 h. **E:** immunoblotting assay. All cells were treated with 0/0.3  $\mu$ g/ml dox for 16 h. **F:** the nSREBP2 expression-induced LDH release in WT and PANX1-deficient HeLa-pTet-nSREBP2 cells. Data are presented as means  $\pm$  SD. Statistical analyses, unpaired two-tailed Student's *t* test. **G:** representative confocal images of PI-stained WT and PANX1-deficient HeLa-pTet-nSREBP2 cells. All cells were induced by 0/0.3  $\mu$ g/ml dox

ABCDE-5KO, *MLKL-KO*, and ABCDEM-6KO cells, resembling that of WT HeLa cells (Fig. 5E and supplemental Video S5). These results excluded the possibility that the canonical membrane-disrupting proteins were the executioner of cell lysis upon nSREBP2 expression.

### PANX1 is critical for nSREBP2-induced membrane rupture

To identify effector proteins that directly permeabilize cell membranes in the context of nSREBP2 overexpression, we carried out whole-genome CRISPR screening using a Toronto human knockout pooled library covering 18,053 coding genes (42). We performed the screening on caspase-3-deficient HeLa cells. Lentiviral particles encoding gRNAs were generated and used for transducing cells with a low MOI (0.3). Cells were then gated with EGFP<sup>+</sup> and PI<sup>-</sup> to enrich resistant cells to nSREBP2-induced cell lysis (Fig. 6A). Genomic DNA was isolated from sorted cells to amplify gRNA cassettes for sequencing. A cluster of gRNAs targeting anti-apoptotic genes were highly enriched, including *caspase-7*, *BCL2 associated X (BAX)*, and *apoptotic peptidase activating factor 1 (APAF1)*, which were essential components of the canonical apoptotic pathway (52, 53), reiterating previous observation of cytochrome C release (Fig. 6B, C). Indeed, transduction of APAF1 gRNA, which led to about 80 percent down-regulation of APAF1 protein, largely inhibited LDH release after nSREBP2 induction (Fig. 6D). BAX leads the mitochondrial outer membrane permeabilization. Then, released cytochrome C binds APAF1, thereby forming an apoptosome structure by activating caspase-9. Caspase-9 cleaves the effector caspases, caspase-3 and caspase-7, inducing apoptosis (53).

Interestingly, our screening also identified the anion-permeable channel PANX1. Previous studies demonstrated that PANX1 was cleaved by caspase-3/7 during apoptosis (34, 37). Cleavage of PANX1 by caspase-7 allows the release of ATP and other molecules through the PANX1 pore. To investigate the essentiality of PANX1, we generated a PANX1 knockout cell line and tested its vulnerability to nSREBP2 expression. Knockout of PANX1 did not affect nSREBP2 expression, while the release of LDH was drastically inhibited (Fig. 6E, F). Cells lacking PANX1 showed a delayed morphologic change, such as roundup and shrinkage, and were non-permeable to PI (Fig. 6G, H). Although

PANX1 pore was only permeable to ~1-kDa molecules (35), blockade of PANX1 pore with carbenoxolone (CBX) fully rescued LDH release both in WT or ABCDE-5KO HeLa-pTet-nSREBP2 cells (Fig. 6I). We then tested whether cleavage of PANX1 was sufficient to trigger cell lysis. Inducible expression of a C-terminally truncated PANX1 protein (PANX1- $\Delta$ CTT), which mimicked caspase-3 and caspase-7 cleavages, resulted in the loss of cell viability, cell content release, and positive PI staining. Overexpression of full-length PANX1 had no obvious effect on cell viability (Fig. 6J-L and supplemental Video S6). Expression of nSREBP2 promoted the cleavage of PANX1, generating a C-terminally truncated PANX1, migrating at around 37 kDa in SDS-PAGE (supplemental Fig. S8A). Besides, the knockout of p73 or caspase-3/7 blocked the cleavage of PANX1 (supplemental Fig. S8B, C). These results suggested PANX1 was the downstream effector causing lytic cell death.

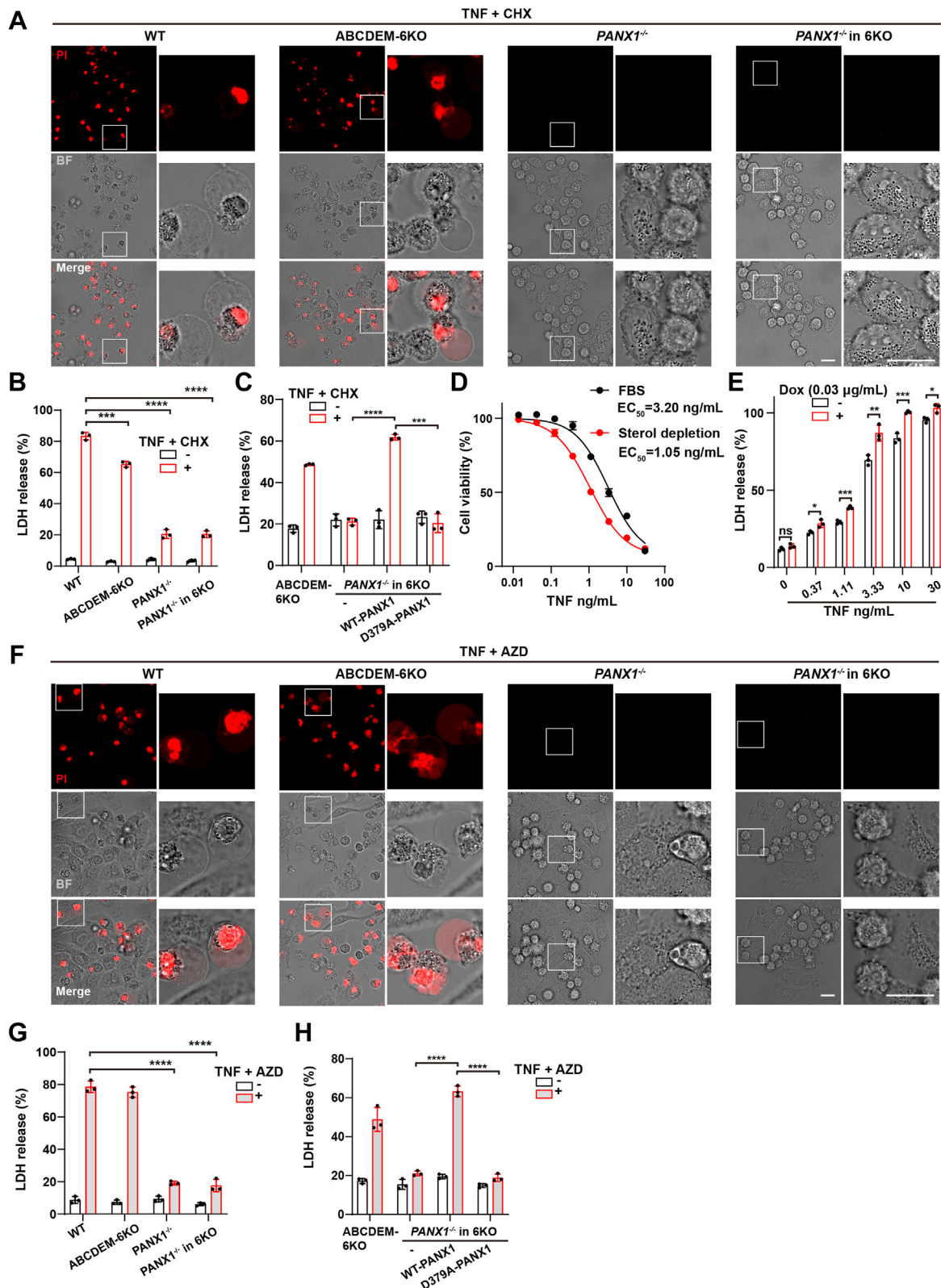
### PANX1 mediates lytic cell death induced by TNF

To explore the role of PANX1-induced cell lysis in a pathophysiological context, we induced HeLa cell death by activating the canonical extrinsic death pathway using tumor necrosis factor (TNF)  $\alpha$  combined with cycloheximide (CHX) (54). Wild-type HeLa-pTet-nSREBP2 cells and the cells lacking gasdermins A-E and MLKL (ABCDEM-6KO) underwent membrane blebbing and were permeable to PI upon TNF/CHX stimulation. In sharp contrast, PANX1-deficient cells were not permeable to PI (Fig. 7A). Concordantly, the released LDH was significantly decreased in PANX1-deficient cells compared with WT and the ABCDEM-6KO cells (Fig. 7B). TNF-mediated lytic cell death was restored by overexpression of wild-type PANX1 but not caspase cleavage site mutant PANX1(D379A) (Fig. 7C). Endogenous SREBP2 activation via sterol starvation sensitized HeLa cells to TNF treatment (Fig. 7D). Besides, low concentration of dox, which mimicked activation level of SREBP2 in sterol-depleted condition, increased LDH release compared to normal condition (Fig. 7E).

Similarly, SMAC mimetic AZD5582 (AZD) targets inhibitors of apoptosis proteins (IAPs) to induce TNF-mediated cell death (55, 56). Membrane extrusion and positive PI staining was only observed in WT cells and ABCDEM-6KO cells treated with TNF plus AZD for 24 h, whereas the cells lacking PANX1 displayed

---

for 36 h, then imaged at 63 $\times$  magnification with 10  $\mu$ g/ml PI. Scale bar, 25  $\mu$ m. H: flow cytometry of PI-stained WT and PANX1-deficient HeLa-pTet-nSREBP2 cells. I: effect of CBX on dox-induced lytic cell death was analyzed by LDH test. WT and ABCDE-5KO HeLa-pTet-nSREBP2 cells were treated with 0/0.3  $\mu$ g/ml dox and 50  $\mu$ M CBX for 36 h. J, Effects of overexpression of PANX1 on cell death. Full length (FL) or truncated ( $\Delta$ CTT) PANX1 in HeLa-pTet-nSREBP2 cells were induced for 24 h by 2  $\mu$ g/ml dox. Cell viability was analyzed by cell counting kit-8. K, LDH release test on the HeLa cells expressing full length (FL) or truncated ( $\Delta$ CTT) PANX1. Cells were treated with or without CBX and dox for 36 h. l, Representative images of truncated ( $\Delta$ CTT) PANX1-expressing HeLa cells under dox induction. Cells were treated with 2  $\mu$ g/ml dox for 24 h, then preloaded with 10  $\mu$ g/ml PI and imaged at 63 $\times$  magnification at 5 min intervals for 12 h. Real-time videos are included in supplemental Video S6. Scale bar, 25  $\mu$ m. \*\*\* $P$  < 0.001. \*\*\*\* $P$  < 0.0001. ND, not detected.



**Fig. 7.** PANX1 promotes gasdermins and MLKL-independent cell lysis during TNF-induced cell death. A: representative images of WT, ABCDEM-6KO, PANX1-deficient, and PANX1-deficient in 6KO HeLa-pTet-nSREBP2 cell treated with 50 ng/ml TNF and 10 μg/ml CHX for 24 h. Scale bar, 25 μm. B: LDH release test. Data are presented as means ± SD. Statistical analyses, unpaired two-tailed Student's *t* test. C: *PANX1* knockout in ABCDEM-6KO HeLa-pTet-nSREBP2 cells were transfected with wild-type or mutated PANX1 (D379A). All cells were treated with TNF and CHX for 24 h. LDH tests were applied to analyze lytic cell death. Data are presented as means ± SD. Statistical analyses, unpaired two-tailed Student's *t* test. D: cell viability test. HeLa cells were plated in 10% FBS medium or sterol depletion medium (5% lipoprotein-deficient serum, 1 μM lovastatin, 10 μM mevalonate) for 16 h, then treated with indicated concentrations of TNF (starting from 30 ng/ml, with 3-fold serial dilutions) and 10 μg/ml CHX for 8 h. Cell viabilities

delayed apoptotic phenotype without membrane rupture (Fig. 7F). Comparing with WT and ABCDEM-6KO cells, the level of released LDH was significantly decreased in PANX1-deficient cells treated with TNF plus AZD and restored by wild-type PANX1 (Fig. 7G, H). These results support the idea that the C-terminal cleaved PANX1 acts as a determinant fact for lytic cell death.

### PANX1 mediates chemotherapy drugs-induced lytic cell death

PANX1 could be the primary mediator of chemotherapy-induced pyroptosis when GSDME was insufficient or blocked (57). We wondered whether PANX1 could mediate cell death induced by different chemotherapy drugs when all gasdermins were deleted. The WT cells and ABCDEM-6KO cells that lack all gasdermins and MLKL underwent lytic cell death and were permeable to PI when treated with doxorubicin or cisplatin. In contrast, deletion of PANX1 abrogated the balloon-like membrane extrusions and PI staining but kept apoptotic responses to doxorubicin or cisplatin (Fig. 8A, B). LDH release were similar in WT and ABCDEM-6KO cells but blunted in PANX1-deficient cells (Fig. 8C). WT PANX1 but not the D379A mutant form of PANX1 restored LDH release in the PANX1 deficient cells (Fig. 8D, E). Similar to TNF treatment, activation of SREBP2 through sterol deprivation or sublethal doxycycline increased the sensitivity to doxorubicin (Fig. 8F, G).

Taken together, our study demonstrated a novel role of SREBP2 to initiate programmed cell death. As illustrated in Fig. 8H, SREBP2 transcriptionally activates p73, promotes apoptotic gene expression, and induces mitochondrial cytochrome C release. Subsequent activation of initiator caspases and executioner caspases led to cleavage of PANX1, promoting pore formation and eventually membrane rupture. Our finding reveals a lytic cell death process which is independent of canonical metabolic functions of SREBP and expands the mechanistic insight of programmed cell death.

## DISCUSSION

The lipogenic regulatory functions of SREBPs have been extensively studied since their discovery in the early 1990's. In this study, we find that overexpression of nSREBP induces lytic cell death. Although we do not have direct evidence showing that this nSREBP-induced cell death exists in vivo, the phenotypes from several

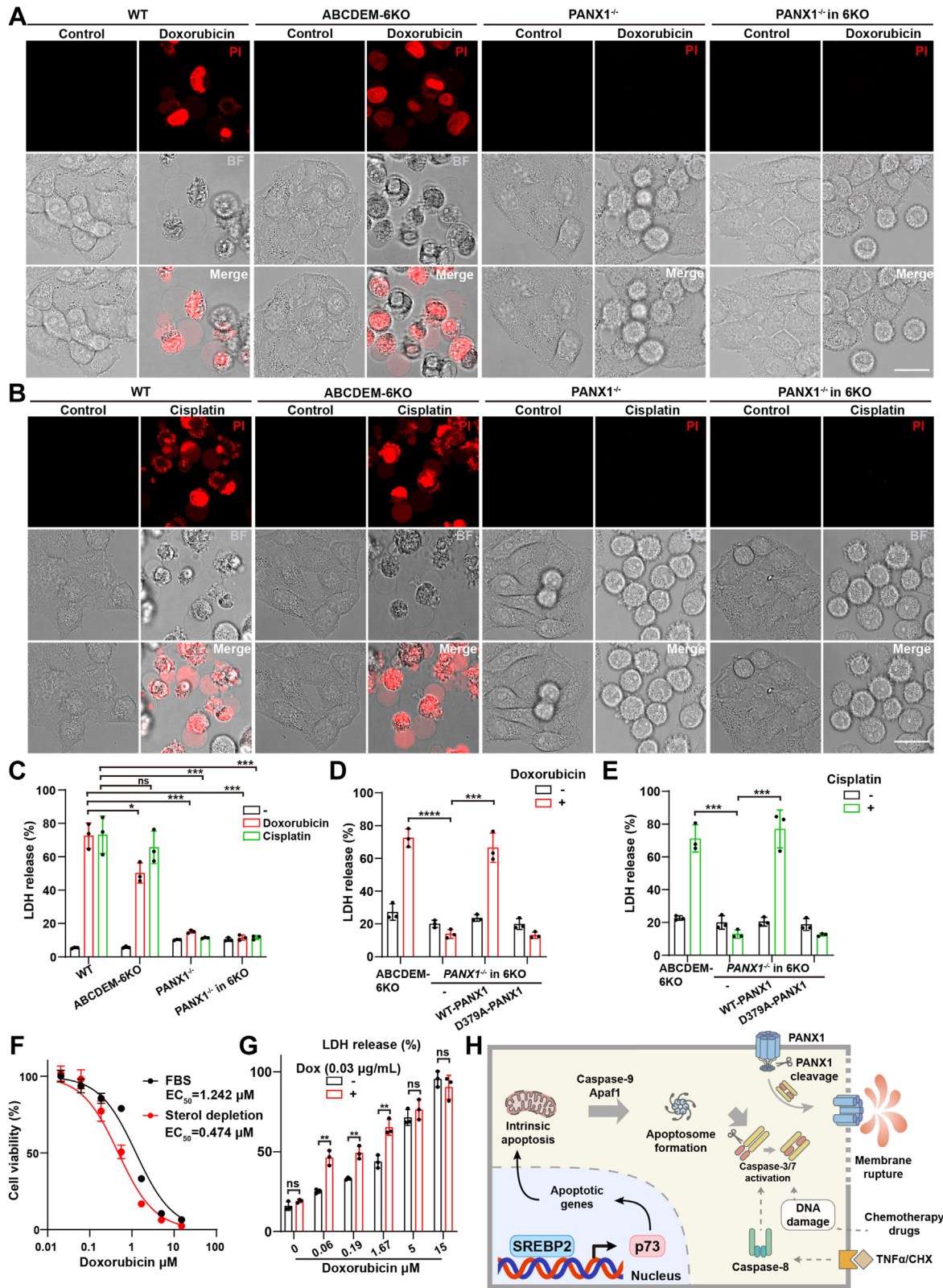
strains of SREBP transgenic mouse models support our finding. For example, mice with overexpressed nSREBP1c in adipocytes displayed reduced cell size in white adipose tissue and a number of immature adipocytes. Histological analysis of white and brown adipose tissue showed signs of inflammation and upregulated TNF levels (58). Transgenic overexpression of nSREBP1a under phosphoenolpyruvate carboxykinase (PEPCK) promoter impaired adipocyte differentiation and increased inflammation in the epididymal WATs of genetically obese mice (59). Similarly, in a series of transgenic mouse models where nSREBPs were under the control of insulin promoter to drive pancreatic  $\beta$  cell-specific expression, the size of islets from transgenic mice was fewer and smaller. The researcher also emphasized that only low expressor strains could be established, implying the lethality by a high level of nSREBPs overexpression (60, 61).

The nSREBPs can contribute to the immune response in various physiological conditions. Tumor necrosis factor (TNF) activated SREBP2 in macrophages. Transcriptomic analysis revealed that SREBP2-controlled cholesterol synthesis pathway was most significantly enriched in primary human macrophages exposed to TNF for 24 h. Adenovirus-mediated transduction of nSREBP2 in macrophages increased the expression of interferon (IFN) regulated genes, such as *CXCL10* and *CXCL11* and sensitized macrophages upon TNF stimulation. Activation of SREBP2 augmented TNF-mediated macrophage activation and inflammatory response and delayed wound healing (62). Recent studies highlight the pro-inflammatory role of SREBPs in myeloid cells. SCAP activation sensitized THP-1 cells to LPS-induced inflammation (63). SREBPs are activated during certain virus or bacterial infections in some clinical settings. Peripheral blood mononuclear cells from COVID-19 patients showed upregulated SREBP2, and the downstream inflammatory responses were positively correlated with the severity of disease. SREBP2 inhibition in mouse models suppressed cytokine storms and pulmonary damages (64). We hypothesize that SREBP-induced lytic cell death might happen in these events and the release of DAMPs aggravates inflammatory responses.

Elevated cholesterol synthesis caused by nSREBP2 activation used to be regarded as the risk of lipotoxicity. Cholesterol overloading induces mitochondria-initiated apoptosis in smooth muscle cells, which promotes necrosis in atherosclerotic lesions (44). Accumulated cholesterol releases mitochondrial DNA and leads to

---

were determined by CCK8 and normalized to CHX only groups. Nonlinear regression was performed in Prism and EC<sub>50</sub> was calculated. E: LDH release test. HeLa-pTet-nSREBP2 cells were plated with 0/0.03  $\mu$ g/ml dox for 8 h, then treated with indicated TNF and 10  $\mu$ g/ml CHX for 8 h. F: representative images of WT, ABCDEM-6KO, PANX1-deficient, and PANX1-deficient in 6KO cell treated with TNF and AZD5582 for 24 h, cells were preloaded with PI for 15 min and imaged at 63 $\times$  magnification. Scale bar, 25  $\mu$ m. G: LDH release test. H: PANX1-deficient in ABCDEM-6KO HeLa-pTet-nSREBP2 cells were transfected with wild-type or mutated PANX1 (D379A). All cells were treated with 50 ng/ml TNF and 5  $\mu$ M AZD5582 for 24 h. LDH tests were applied to analyze lytic cell death. Data are presented as means  $\pm$  SD. Statistical analyses, unpaired two-tailed Student's *t* test. \**P* < 0.05, \*\**P* < 0.01, \*\*\**P* < 0.001, \*\*\*\**P* < 0.0001. ns, not significant.



**Fig. 8.** PANX1 mediates chemotherapy drugs-induced lytic cell death independent of gasdermins and MLKL. **A:** Representative images of WT, ABCDEM-6KO, PANX1-deficient, and PANX1-deficient in 6KO HeLa-pTet-nSREBP2 cell treated with or without 10  $\mu$ M doxorubicin or 30  $\mu$ M cisplatin for 24 h. Cells were preloaded with PI for 15 min and imaged at 63 $\times$  magnification. Scale bar, 25  $\mu$ m. **B:** representative images of ABCDEM-6KO and PANX1-deficient in 6KO HeLa-pTet-nSREBP2 cell treated with or without cisplatin for 24 h. Scale bar, 25  $\mu$ m. **C:** LDH release test. Data are presented as means  $\pm$  SD. Statistical analyses, unpaired two-tailed Student's *t* test. **D** and **E:** the ABCDEM-6KO and PANX1-deficient HeLa-pTet-nSREBP2 cells were transfected with a plasmid expressing wild-type or mutated PANX1 (D379A). All cells were treated with doxorubicin (**D**) or cisplatin (**E**) for 24 h. Data are presented as means  $\pm$  SD. Statistical analyses, unpaired two-tailed Student's *t* test. **F:** cell viability test. HeLa cells were plated in 10%

caspase-1-dependent inflammasome activation in LPS-exposed cholesterol-25-hydroxylase knockout macrophages (65). In our settings, however, inhibition of de novo cholesterol synthesis or depletion of intracellular cholesterol by cyclodextrin do not prevent SREBP2-mediated cell death, suggesting that the over-expression of nSREBP2-induced cell death is independent of lipid biosynthesis. Our data indicate that nSREBP2-induced p73 signaling is the major mechanism to drive lytic cell death. The nSREBP2 causes the release of cytochrome C that activates the formation of apoptosome. Knockdown of TAp73 reduces caspase-9, the key constitutional protein of apoptosome. Consistently, previous studies have shown that TAp73 acts as a tumor suppressor by triggering apoptosis, DNA repair, and autophagy (49, 66). It is also known that the chemotherapy drugs, cisplatin and doxorubicin, can stimulate the phosphorylation of TAp73 by cellular Abelson leukemia (c-Abl) kinase and promote TAp73-dependent apoptosis (67, 68).


Gasdermin-mediated pyroptosis is a form of pro-inflammatory lytic cell death. Gasdermins undergo proteolytic processing by caspases to generate truncated N-terminal domains, which oligomerize to permeabilize cell membranes. PANX1 is cleaved by caspase-3 or -7, generating a C-terminal truncated form that releases ATP. Released ATP binds to P2X7 on plasma membrane and triggers cytolysis (69). Besides well-known gasdermins and MLKL, a recent report found that nerve injury-induced protein1 (NINJ1) was essential for inducing plasma membrane rupture. *Ninj1*<sup>-/-</sup> macrophages maintained plasma membrane integrity throughout the stages of pyroptosis, necroptosis and apoptosis, and dying *Ninj1*<sup>-/-</sup> macrophages exhibited persistent balloon-like morphology and LDH release (70). In this study, we demonstrate that PANX1 can promote lytic cell death independent of P2X7 or NINJ1 (supplemental Fig. S9). It is known that PANX1 mediates chemotherapy-induced lytic cell death independent of GSDME (57, 71). Our findings further demonstrate that PANX1 promotes lytic cell death independent of any other known pore-forming proteins including gasdermins, MLKL, P2X7, and NINJ1.

The expression level of nSREBP to induce lytic cell death is much higher than that of sterol-depletion-induced nSREBP. Therefore, the nSREBP-induced cell death could be questioned as an artificial phenomenon. However, sterol depletion-induced SREBP2 activation increased cell sensitivity to chemotherapy drugs or TNF, suggesting the physiological significance of our finding. Moreover, induction of cell death usually

requires extreme conditions. Typical examples include apoptosis induction by TNF and cycloheximide, and necroptosis by the combination of TNF, Smac mimetic, and z-VAD. Such manipulation advanced our understanding of the regulatory mechanisms of programmed cell death.

In summary, this study reports that nSREBP2 induces p73-dependent lytic cell death. Activation of caspase cascade cleaves PANX1 to promote membrane rupture. Further studies are required to illustrate the in vivo pathophysiological importance of this process.

### Data availability

All data are included in the article and supplemental information, and all data used in the article are available from the corresponding author upon reasonable request. 

### Supplemental data

This article contains [supplemental data](#).



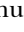

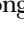
### Acknowledgment

We thank Dr Feng Shao (National institute of biological sciences, China) and Dr Hai Jiang (Center for Excellence in Molecular Cell Science, China) for providing plasmids.

### Author contributions

W.-Z. Z. and Z.-Y. H. resources; W.-Z. Z. methodology; A. H. validation; A. H., Y. X., Z.-Y. H., and J. L. investigation. Y. X. and B.-L. S. writing-review & editing; Y. X. and B.-L. S. writing-original draft; B.-L. S. project administration; B.-L. S. funding acquisition; B.-L. S., Z.-Y. H., and J. L. data curation; B.-L. S. conceptualization.

### Author ORCIDs

Yanni Xiong  <https://orcid.org/0000-0002-1777-4999>  
Zi-Yun Hong  <https://orcid.org/0009-0006-8176-7036>  
Wen-Zhuo Zhu  <https://orcid.org/0009-0004-0274-8108>  
Ao Hu  <https://orcid.org/0000-0001-5763-204X>  
Bao-Liang Song  <https://orcid.org/0000-0002-6397-5935>

### Funding and additional information

This work was supported by grants from Ministry of Science and Technology of China (2018YFA0800700) and the National Natural Science Foundation of China (92354301, 91954203, 32021003). B.-L. S. acknowledges the support from the Tencent Foundation through the XPLOER PRIZE.

### Conflict of interest

The authors declare that they have no conflicts of interest with the contents of this article.

FBS medium or sterol depletion medium (5% lipoprotein-deficient serum, 1  $\mu$ M lovastatin, 10  $\mu$ M mevalonate) for 16 h, then treated with indicated concentrations of doxorubicin (starting from 15  $\mu$ M, with 3-fold serial dilutions) for 24 h. Nonlinear regression was performed in Prism and EC<sub>50</sub> was calculated. G: LDH release test. HeLa-pTet-nSREBP2 cells were plated with 0/0.03  $\mu$ g/ml doxycycline for 8 h, then treated with indicated doxorubicin for 24 h. H, Proposed model of nSREBP2 induced lytic cell death. \* $P < 0.05$ , \*\* $P < 0.001$ , \*\*\* $P < 0.0001$ . ns, not significant.



## Abbreviations

APAF1, apoptotic peptidase activating factor 1; CBX, carbinoxolone; CHX, cycloheximide; LDH, lactate dehydrogenase; LPS, lipopolysaccharide; MLKL, mixed lineage kinase domain-like; NINJ1, nerve injury-induced protein1; PANX1, pannexin-1; PI, propidium iodide; PS, phosphatidylserine; SCAP, SREBP-cleavage activating protein; TNF, tumor necrosis factor.

Manuscript received April 1, 2024, and in revised form June 6, 2024. Published, JLR Papers in Press, June 14, 2024, <https://doi.org/10.1016/j.jlr.2024.100579>

## REFERENCES

- Goldstein, J. L., DeBose-Boyd, R. A., and Brown, M. S. (2006) Protein sensors for membrane sterols. *Cell* **124**, 35–46
- Luo, J., Yang, H., and Song, B. L. (2020) Mechanisms and regulation of cholesterol homeostasis. *Nat. Rev. Mol. Cell Biol.* **21**, 225–245
- Horton, J. D., Shah, N. A., Warrington, J. A., Anderson, N. N., Park, S. W., Brown, M. S., *et al.* (2003) Combined analysis of oligonucleotide microarray data from transgenic and knockout mice identifies direct SREBP target genes. *Proc. Natl. Acad. Sci. U. S. A.* **100**, 12027–12032
- Amemiya-Kudo, M., Shimano, H., Hastay, A. H., Yahagi, N., Yoshikawa, T., Matsuzaka, T., *et al.* (2002) Transcriptional activities of nuclear SREBP-1a, -1c, and -2 to different target promoters of lipogenic and cholesterologenic genes. *J. Lipid Res.* **43**, 1220–1235
- Horton, J. D., Goldstein, J. L., and Brown, M. S. (2002) SREBPs: activators of the complete program of cholesterol and fatty acid synthesis in the liver. *J. Clin. Invest.* **109**, 1125–1131
- Nakakuki, M., Shimano, H., Inoue, N., Tamura, M., Matsuzaka, T., Nakagawa, Y., *et al.* (2007) A transcription factor of lipid synthesis, sterol regulatory element-binding protein (SREBP)-1a causes G1 cell-cycle arrest after accumulation of cyclin-dependent kinase (cdk) inhibitors. *FEBS J.* **274**, 4440–4452
- Shao, W., and Espenshade, P. J. (2012) Expanding roles for SREBP in metabolism. *Cell Metab.* **16**, 414–419
- Xiao, J., Xiong, Y., Yang, L. T., Wang, J. Q., Zhou, Z. M., Dong, L. W., *et al.* (2021) POST1/C12ORF49 regulates the SREBP pathway by promoting site-1 protease maturation. *Protein Cell* **12**, 279–296
- Van Rooyen, D. M., Larter, C. Z., Haigh, W. G., Yeh, M. M., Ioannou, G., Kuver, R., *et al.* (2011) Hepatic free cholesterol accumulates in obese, diabetic mice and causes nonalcoholic steatohepatitis. *Gastroenterology* **141**, 1393–1403
- Min, H. K., Kapoor, A., Fuchs, M., Mirshahi, F., Zhou, H., Maher, J., *et al.* (2012) Increased hepatic synthesis and dysregulation of cholesterol metabolism is associated with the severity of nonalcoholic fatty liver disease. *Cell Metab.* **15**, 665–674
- Caballero, F., Fernandez, A., De Lacy, A. M., Fernandez-Checa, J. C., Caballeria, J., and Garcia-Ruiz, C. (2009) Enhanced free cholesterol, SREBP-2 and StAR expression in human NASH. *J. Hepatol.* **50**, 789–796
- Jiang, S. Y., Yang, X., Yang, Z., Li, J. W., Xu, M. Q., Qu, Y. X., *et al.* (2022) Discovery of an insulin-induced gene binding compound that ameliorates nonalcoholic steatohepatitis by inhibiting sterol regulatory element-binding protein-mediated lipogenesis. *Hepatology* **76**, 1466–1481
- Tang, J. J., Li, J. G., Qi, W., Qiu, W. W., Li, P. S., Li, B. L., *et al.* (2011) Inhibition of SREBP by a small molecule, betulin, improves hyperlipidemia and insulin resistance and reduces atherosclerotic plaques. *Cell Metab.* **13**, 44–56
- Moon, Y. A., Liang, G., Xie, X., Frank-Kamenetsky, M., Fitzgerald, K., Kotliansky, V., *et al.* (2012) The Scap/SREBP pathway is essential for developing diabetic fatty liver and carbohydrate-induced hypertriglyceridemia in animals. *Cell Metab.* **15**, 240–246
- Brown, M. S., and Goldstein, J. L. (2012) Scientific side trips: six excursions from the beaten path. *J. Biol. Chem.* **287**, 22418–22435
- Seo, Y. K., Jeon, T. I., Chong, H. K., Biesinger, J., Xie, X., and Osborne, T. F. (2011) Genome-wide localization of SREBP-2 in hepatic chromatin predicts a role in autophagy. *Cell Metab.* **13**, 367–375
- Xiao, H., Lu, M., Lin, T. Y., Chen, Z., Chen, G., Wang, W. C., *et al.* (2013) Sterol regulatory element binding protein 2 activation of NLRP3 inflammasome in endothelium mediates hemodynamic-induced atherosclerosis susceptibility. *Circulation* **128**, 632–642
- Im, S. S., Yousef, L., Blaschitz, C., Liu, J. Z., Edwards, R. A., Young, S. G., *et al.* (2011) Linking lipid metabolism to the innate immune response in macrophages through sterol regulatory element binding protein-1a. *Cell Metab.* **13**, 540–549
- Silva, M. T., do Vale, A., and dos Santos, N. M. (2008) Secondary necrosis in multicellular animals: an outcome of apoptosis with pathogenic implications. *Apoptosis* **13**, 463–482
- Silva, M. T. (2010) Bacteria-induced phagocyte secondary necrosis as a pathogenicity mechanism. *J. Leukoc. Biol.* **88**, 885–896
- Silva, M. T. (2010) Secondary necrosis: the natural outcome of the complete apoptotic program. *FEBS Lett.* **584**, 4491–4499
- Vanden Berghe, T., Vanlangenakker, N., Parthoens, E., Deckers, W., Devos, M., Festjens, N., *et al.* (2010) Necroptosis, necrosis and secondary necrosis converge on similar cellular disintegration features. *Cell Death Differ.* **17**, 922–930
- Rogers, C., Fernandes-Alnemri, T., Mayes, L., Alnemri, D., Cingolani, G., and Alnemri, E. S. (2017) Cleavage of DFNA5 by caspase-3 during apoptosis mediates progression to secondary necrotic/pyroptotic cell death. *Nat. Commun.* **8**, 14128
- Zhang, Y., Chen, X., Gueydan, C., and Han, J. (2018) Plasma membrane changes during programmed cell deaths. *Cell Res.* **28**, 9–21
- Shi, J., Zhao, Y., Wang, K., Shi, X., Wang, Y., Huang, H., *et al.* (2015) Cleavage of GSDMD by inflammatory caspases determines pyroptotic cell death. *Nature* **526**, 660–665
- Ding, J., Wang, K., Liu, W., She, Y., Sun, Q., Shi, J., *et al.* (2016) Pore-forming activity and structural autoinhibition of the gasdermin family. *Nature* **535**, 111–116
- Wang, Y., Gao, W., Shi, X., Ding, J., Liu, W., He, H., *et al.* (2017) Chemotherapy drugs induce pyroptosis through caspase-3 cleavage of a gasdermin. *Nature* **547**, 99–103
- Wang, Q., Wang, Y., Ding, J., Wang, C., Zhou, X., Gao, W., *et al.* (2020) A bioorthogonal system reveals antitumour immune function of pyroptosis. *Nature* **579**, 421–426
- Wang, H., Sun, L., Su, L., Rizo, J., Liu, L., Wang, L. F., *et al.* (2014) Mixed lineage kinase domain-like protein MLKL causes necrotic membrane disruption upon phosphorylation by RIP3. *Mol. Cell* **54**, 133–146
- Derangere, V., Chevriaux, A., Courtaut, F., Bruchard, M., Berger, H., Chalmin, F., *et al.* (2014) Liver X receptor beta activation induces pyroptosis of human and murine colon cancer cells. *Cell Death Differ.* **21**, 1914–1924
- Yang, D., He, Y., Munoz-Planillo, R., Liu, Q., and Nunez, G. (2015) Caspase-1 requires the pannexin-1 channel and the purinergic P2X7 pore to mediate pyroptosis and endotoxin shock. *Immunity* **43**, 923–932
- Crespo Yanguas, S., Willebrords, J., Johnstone, S. R., Maes, M., Decrock, E., De Bock, M., *et al.* (2017) Pannexin1 as mediator of inflammation and cell death. *Biochim. Biophys. Acta Mol. Cell Res.* **1864**, 51–61
- Pelegrin, P., and Surprenant, A. (2007) Pannexin-1 couples to maitotoxin- and nigericin-induced interleukin-1 $\beta$  release through a dye uptake-independent pathway. *J. Biol. Chem.* **282**, 2386–2394
- Chekeni, F. B., Elliott, M. R., Sandilos, J. K., Walk, S. F., Kinchen, J. M., Lazarowski, E. R., *et al.* (2010) Pannexin 1 channels mediate 'find-me' signal release and membrane permeability during apoptosis. *Nature* **467**, 863–867
- Ruan, Z., Orozco, I. J., Du, J., and Lu, W. (2020) Structures of human pannexin 1 reveal ion pathways and mechanism of gating. *Nature* **584**, 646–651
- Zamaraeva, M. V., Sabirov, R. Z., Maeno, E., Ando-Akatsuka, Y., Bessonova, S. V., and Okada, Y. (2005) Cells die with increased cytosolic ATP during apoptosis: a bioluminescence study with intracellular luciferase. *Cell Death Differ.* **12**, 1390–1397
- Sandilos, J. K., Chiu, Y. H., Chekeni, F. B., Armstrong, A. J., Walk, S. F., Ravichandran, K. S., *et al.* (2012) Pannexin 1, an ATP release channel, is activated by caspase cleavage of its pore-associated C-terminal autoinhibitory region. *J. Biol. Chem.* **287**, 11303–11311
- Munoz-Planillo, R., Kuffa, P., Martinez-Colon, G., Smith, B. L., Rajendiran, T. M., and Nunez, G. (2013) K(+) efflux is the

- common trigger of NLRP3 inflammasome activation by bacterial toxins and particulate matter. *Immunity*. **38**, 1142–1153
39. Goldstein, J. L., Basu, S. K., and Brown, M. S. (1983) Receptor-mediated endocytosis of low-density lipoprotein in cultured cells. *Methods Enzymol.* **98**, 241–260
  40. Redgrave, T. G., Roberts, D. C., and West, C. E. (1975) Separation of plasma lipoproteins by density-gradient ultracentrifugation. *Anal. Biochem.* **65**, 42–49
  41. Hu, A., Zhang, J. Z., Wang, J., Li, C. C., Yuan, M., Deng, G., *et al.* (2022) Cholesterylation of Smoothed is a calcium-accelerated autoreaction involving an intramolecular ester intermediate. *Cell Res.* **32**, 288–301
  42. Hart, T., Chandrashekhar, M., Aregger, M., Steinhart, Z., Brown, K. R., MacLeod, G., *et al.* (2015) High-resolution CRISPR screens reveal fitness genes and genotype-specific cancer liabilities. *Cell*. **163**, 1515–1526
  43. Castellino, R. C., De Bortoli, M., Lin, L. L., Skapura, D. G., Rajan, J. A., Adesina, A. M., *et al.* (2007) Overexpressed TP73 induces apoptosis in medulloblastoma. *BMC cancer*. **7**, 127
  44. Kedi, X., Ming, Y., Yongping, W., Yi, Y., and Xiaoxiang, Z. (2009) Free cholesterol overloading induced smooth muscle cells death and activated both ER- and mitochondrial-dependent death pathway. *Atherosclerosis*. **207**, 123–130
  45. Shu, F., Chen, J., Ma, X., Fan, Y., Yu, L., Zheng, W., *et al.* (2018) Cholesterol crystal-mediated inflammation is driven by plasma membrane destabilization. *Front. Immunol.* **9**, 1163
  46. Dang, C. V. (2012) MYC on the path to cancer. *Cell*. **149**, 22–35
  47. Vikhrev, P., Melino, G., and Amelio, I. (2018) p73 alternative splicing: exploring a biological role for the C-terminal isoforms. *J. Mol. Biol.* **430**, 1829–1838
  48. Dotsch, V., Bernassola, F., Coutandin, D., Candi, E., and Melino, G. (2010) p63 and p73, the ancestors of p53. *Cold Spring Harb. Perspect. Biol.* **2**, a004887
  49. Ramos, H., Raimundo, L., and Saraiva, L. (2020) p73: from the p53 shadow to a major pharmacological target in anticancer therapy. *Pharmacol. Res.* **162**, 105245
  50. Tang, D., Kang, R., Berghe, T. V., Vandennebe, P., and Kroemer, G. (2019) The molecular machinery of regulated cell death. *Cell Res.* **29**, 347–364
  51. Tait, S. W., and Green, D. R. (2010) Mitochondria and cell death: outer membrane permeabilization and beyond. *Nat. Rev. Mol. Cell Biol.* **11**, 621–632
  52. Twiddy, D., Cohen, G. M., Macfarlane, M., and Cain, K. (2006) Caspase-7 is directly activated by the approximately 700-kDa apoptosome complex and is released as a stable XIAP-caspase-7 approximately 200-kDa complex. *J. Biol. Chem.* **281**, 3876–3888
  53. Bao, Q., and Shi, Y. (2007) Apoptosome: a platform for the activation of initiator caspases. *Cell Death Differ.* **14**, 56–65
  54. Miura, M., Friedlander, R. M., and Yuan, J. (1995) Tumor necrosis factor-induced apoptosis is mediated by a CrmA-sensitive cell death pathway. *Proc. Natl. Acad. Sci. U. S. A.* **92**, 8318–8322
  55. Vince, J. E., Wong, W. W., Gentle, I., Lawlor, K. E., Allam, R., O'Reilly, L., *et al.* (2012) Inhibitor of apoptosis proteins limit RIP3 kinase-dependent interleukin-1 activation. *Immunity*. **36**, 215–227
  56. Fulda, S. (2015) Promises and challenges of smac mimetics as cancer therapeutics. *Clin. Cancer Res.* **21**, 5030–5036
  57. Zhou, B., Ryder, C. B., Dubyak, G. R., and Abbott, D. W. (2022) Gasdermins and pannexin-1 mediate pathways of chemotherapy-induced cell lysis in hematopoietic malignancies. *Sci. Signal.* **15**, eabl6781
  58. Shimomura, I., Hammer, R. E., Richardson, J. A., Ikemoto, S., Bashmakov, Y., Goldstein, J. L., *et al.* (1998) Insulin resistance and diabetes mellitus in transgenic mice expressing nuclear SREBP-1c in adipose tissue: model for congenital generalized lipodystrophy. *Genes Dev.* **12**, 3182–3194
  59. Ohno, H., Matsuzaka, T., Tang, N., Sharma, R., Motomura, K., Shimura, T., *et al.* (2018) Transgenic mice overexpressing SREBP-1a in male ob/ob mice exhibit lipodystrophy and exacerbate insulin resistance. *Endocrinology*. **159**, 2308–2323
  60. Ishikawa, M., Iwasaki, Y., Yatoh, S., Kato, T., Kumadaki, S., Inoue, N., *et al.* (2008) Cholesterol accumulation and diabetes in pancreatic beta-cell-specific SREBP-2 transgenic mice: a new model for lipotoxicity. *J. Lipid Res.* **49**, 2524–2534
  61. Takahashi, A., Motomura, K., Kato, T., Yoshikawa, T., Nakagawa, Y., Yahagi, N., *et al.* (2005) Transgenic mice overexpressing nuclear SREBP-1c in pancreatic beta-cells. *Diabetes*. **54**, 492–499
  62. Kusanadi, A., Park, S. H., Yuan, R., Pannellini, T., Giannopoulou, E., Oliver, D., *et al.* (2019) The cytokine TNF promotes transcription factor SREBP activity and binding to inflammatory genes to activate macrophages and limit tissue repair. *Immunity*. **51**, 241–257.e249
  63. Ouyang, N., Gan, H., He, Q., Lei, H., Wang, S. Y., Liu, Q., *et al.* (2018) Dysfunction of cholesterol sensor SCAP promotes inflammation activation in THP-1 macrophages. *Exp. Cell Res.* **367**, 162–169
  64. Lee, W., Ahn, J. H., Park, H. H., Kim, H. N., Kim, H., Yoo, Y., *et al.* (2020) COVID-19-activated SREBP2 disturbs cholesterol biosynthesis and leads to cytokine storm. *Signal. Transduct. Target. Ther.* **5**, 186
  65. Dang, E. V., McDonald, J. G., Russell, D. W., and Cyster, J. G. (2017) Oxysterol restraint of cholesterol synthesis prevents AIM2 inflammasome activation. *Cell*. **171**, 1057–1071.e1011
  66. Stiewe, T., and Putzer, B. M. (2002) Role of p73 in malignancy: tumor suppressor or oncogene? *Cell Death Differ.* **9**, 237–245
  67. Agami, R., Blandino, G., Oren, M., and Shaul, Y. (1999) Interaction of c-Abl and p73alpha and their collaboration to induce apoptosis. *Nature*. **399**, 809–813
  68. Gong, J. G., Costanzo, A., Yang, H. Q., Melino, G., Kaelin, W. G., Jr., Levrero, M., *et al.* (1999) The tyrosine kinase c-Abl regulates p73 in apoptotic response to cisplatin-induced DNA damage. *Nature*. **399**, 806–809
  69. Pelegrin, P., and Surprenant, A. (2006) Pannexin-1 mediates large pore formation and interleukin-1beta release by the ATP-gated P2X7 receptor. *EMBO J.* **25**, 5071–5082
  70. Kayagaki, N., Kornfeld, O. S., Lee, B. L., Stowe, I. B., O'Rourke, K., Li, Q., *et al.* (2021) NINJ1 mediates plasma membrane rupture during lytic cell death. *Nature*. **591**, 131–136
  71. Chen, K. W., Demarco, B., Heilig, R., Shkarina, K., Boettcher, A., Farady, C. J., *et al.* (2019) Extrinsic and intrinsic apoptosis activate pannexin-1 to drive NLRP3 inflammasome assembly. *EMBO J.* **38**, e101638